Tufts UNIVERSITY | School of Engineering

Radial Dependency of Droplet Oscillatory Natural Frequency Shift with Varying Deformation Amplitude

Submitted By
Courtland Priest

IN PARTIAL FULFILLMENT OF THE REQUIREMENTS FOR AN
UNDERGRADUATE HONORS THESIS WITH A

BACHELOR OF SCIENCE IN MECHANICAL ENGINEERING

School of Engineering
Tufts University
Medford, Massachusetts

December 2019

Signature of Author:
Courtland Priest

Thesis Chairman:
Associate Professor Douglas M. Matson
Department of Mechanical Engineering
Tufts University

Committee:
Professor R. Glynn Holt
Department of Mechanical Engineering
Boston University

Abstract

A suggested size dependency of the amplitude-varying shift in damped natural frequency of an oscillating droplet is explored using acoustic levitation techniques. An acoustic levitator facility is configured to facilitate the acquisition of high-fidelity high-speed video imaging data and a program is developed to determine a droplet's frequency over each oscillatory period by measuring the time between deformation maxima and minima. Data acquisition is conducted by driving a droplet near its estimated natural frequency, abruptly removing the forcing modulation and recording the transient behavior as the droplet's oscillations decay due to internal viscous dissipation of kinetic energy.

A tentative correlation between droplet size and the rate at which the natural frequency decreases with increasing amplitude is observed, with smaller droplets exhibiting a greater decrease for a given normalized deformation amplitude. This supports the results of a prior study which was also conducted using acoustic levitation techniques. A secondary study of the effect of acoustic pressure (quantified as resting deformation of a droplet in the acoustic field) on the frequency is conducted but variance in the data is too large to confidently note trends. Two methods of analyzing oscillatory frequency shift data are utilized and their results are compared. Uncertainties both in experimental technique and intrinsic to the utilized hardware and software are characterized to facilitate minimization thereof for further study of the observed size dependency.

Acknowledgments

I extend heartfelt thanks to Robert Priest and Elisa Blanchard, without whose steadfast support this research and the studies leading up to it would never have happened. Further thanks go to Professor R. Glynn Holt of Boston University's Mechanical Engineering Department for the use of his acoustic levitator apparatus and attendant equipment and to Vahideh Ansari Hosseinzadeh for detailed instruction in its operation. Professor Douglas Matson and his research group within Tufts University's Department of Mechanical Engineering have provided plentiful advice, constructive criticism and intellectual resources over the course of this project, and they are also deserving of great thanks. Finally, I will thank all the faculty and staff of the Tufts Mechanical Engineering Department for teaching me how to learn, study, and grow as an engineer and researcher.

This work is partially supported under grant number 80NSSC19K0256 from the NASA ELFSTONE program.

Table of Contents

List of Tables

List of Figures

Nomenclature

A	Amplitude, oscillatory [m]
c	Concentration [units variable]
f	Frequency, oscillatory [Hz]
f_0	Damped natural frequency at zero amplitude [Hz]
l	Spherical harmonic degree
m	Spherical harmonic order
R	Droplet radius
t	Time [s]
u	Velocity [m/s]
v	Volume fraction
V	Droplet volume [m^3]
x	Mole fraction
ρ	Material density [kg/m^3]
τ	Free-decay time constant [s]
μ	Viscosity [Pa s]
σ	Interfacial tension [N/m]
ω	Angular frequency [rad/s]
δ	Deformation parameter [dimensionless]

Introduction

In the development of engineering alloys, a prevalent method for assessing material thermophysical properties relies on suspending a liquid sample of the material under consideration so it contacts no surfaces which could instigate microstructural nucleation and solidification. The suspending force may be derived from electrostatic interaction, magnetism or high-frequency standing pressure waves. A sample droplet may then be excited to oscillate at its natural resonant frequency, and the characteristics of this oscillation in tandem with the sample's physical dimensions permit the assessment of material surface tension and viscosity characteristics.

An oscillating droplet's damped natural frequency dependence on surface tension has been extensively studied, and in a subset of situations a real droplet's motion can be comprehensively described by the effects of surface tension alone. However, the test scenarios where this is not the case are many more than where it is, which is the basis of this thesis along with a library of other works on the subject. Understanding the nonlinear behavior exhibited by real (as opposed to idealized) oscillating droplets is vital to successfully applying levitation techniques to thermophysical property characterization. One such nonlinear phenomenon, often observed and at this point well characterized, is that of a droplet's natural frequency varying with its oscillation amplitude. Some prior research suggests that an additional dependence on the droplet's mass also exists, and since property characterization testing is conducted with a wide range of sample sizes depending on the technique utilized and the material being tested, further resolution of this correlation will improve

the acuity of the corrections used in testing that involves moderate to large deformation amplitudes (a range that includes any deformation of more than a few percent).

The data obtained from property characterization studies is used today to develop computational models for welding, casting and other molten-metal manufacturing processes. These are then employed to produce metal parts which are more homogeneous in composition and microstructure and have reduced rates of failure for aerospace, automotive and myriad other applications. Accurate accounting for nonlinear behaviors introduced by material properties, sample dimensions and testing method must thus be conducted to ensure that the developed models have a minimum of intrinsic systematic error.

Background

Small-Amplitude Linear Oscillations

A correlation between suspended droplet surface tension, physical dimensions and fundamental-mode resonant oscillatory frequency was developed by Lord Rayleigh in 1879 [1]. His experimentation involved the study of jets of liquid through different orifices, the shapes of which he used to modify the oscillatory behavior of the jets which he then observed and theorized upon. Part of his investigation concerned the oscillatory behavior of quasi-spherical droplets as they separated from the jet under capillary forces, and he derived a formulation for their behavior in terms of their size and surface tension. This theoretical treatment assumed the limit of infinitely small deformation and is thus a good model for real oscillatory cases where the amplitude is small. Rayleigh's formula for oscillatory mode $l = 2$ is given below.

$$f_0 = \sqrt{\frac{8\sigma}{3\pi\rho V}} \tag{1}$$

This model breaks down at moderate to large deformations as nonlinear relationships between physical characteristics become nonnegligible. As the magnitude of droplet deformation increases, the natural frequency has been shown to decrease, a result Rayleigh anticipated in a theoretical sense in his 1879 work, but which was not further explored or experimentally verified until nearly a century later.

Nonlinear Inviscid Oscillation Theory

Building on the results of numerical studies conducted by Foote [2] and Alonso [3], Tsamopoulos and Brown developed a formalism for the oscillation of axisymmetric inviscid droplets at moderate amplitudes [4]. This defines a droplet's oscillations at each mode l in terms of its kinetic and surface energy and arrives at, among other things, an analytical basis for a natural frequency that decreases with the square of the deformation. Tsamopoulos and Brown compared their asymptotic result with the handful of numerically obtained datapoints that Foote produced, and found good agreement (less than 10 percent error) for droplets of aspect ratios (width divided by height) of up to 1.8. This was attributed to the relatively inviscid medium Foote chose to run his simulations on; Alonso, who applied a very similar Marker-and-Cell (MAC) numerical method to a droplet with much higher viscosity, observed results which differ significantly from both it and the asymptotic curve of Tsamopoulos and Brown. Foote and Tsamopoulos and Brown are in agreement regarding the shape of droplets in the prolate phase of a large-amplitude oscillation [2], [4]. They indicate that in the case of linear oscillation theory (essentially applying Rayleigh's findings to oscillations of more than infinitely small amplitudes), the prolate droplet's curvature becomes slightly re-entrant; i.e. the droplet takes on a two-lobed aspect. This was not observed either in Tsamopoulos and Brown's asymptotic case or Foote's numerical simulation; they both observed an ellipsoid-like prolate shape with no obvious distribution of volume away from the droplet's middle.

Foote and Tsamopoulos and Brown also identified the likely major contributor to the droplet's nonlinear decrease in natural frequency at high amplitude. The

asymptotic and numerical results both indicate that the droplet spends significantly more time in a prolate shape than in an oblate one. This result is shown to be due to the absence of the two-lobed behavior predicted by the linear Rayleigh model, which reduces the droplet's overall surface area and by extension its surface energy. The qualitative effect of this reduction is a less rapid return to a neutral shape than would be the case in a droplet with purely linear behavior. With the time spent in the oblate phase of the oscillation not experiencing significant change over the course of an oscillatory period, this increase in prolate-phase time represents the bulk of the total increase in oscillatory period of a nonlinearly oscillating droplet.

Oscillation of Viscous Droplets

With real liquids, viscous forces acting within a droplet serve to damp out oscillatory motion in the absence of an external impulse. The rate of this decay for a given oscillatory mode l may be modeled (at least for small deformation amplitudes) by a damped harmonic oscillator, represented analytically by the relation below as given by Becker et al. among others [5].

$$A_l(t) = A_{0,l}e^{-t/\tau} \tag{2}$$

Becker et al. also developed an analytical approximation for the dimensionless deformation a_l of an oscillating droplet as a function of time, which uses this decay rate relation and has been transcribed below [5].

$$a_l(t) = A_l sin\{Nf_l\left[(1-(f_l\tau_l)^{-2})^{1/2} + \alpha_l A_l^2\right]t + \phi_l\} + \beta_l A_l^2 \tag{3}$$

This approximation contains terms which describe almost every factor affecting a droplet's deviation from ideal behavior. As explained by Becker et al., the term with α_l

describes the droplet's oscillatory frequency dependence on deformation amplitude, the term with β_l models the asymmetry between the oblate and prolate deformation amplitudes and ϕ_l is the oscillation's phase angle. This model also takes into account radius change due to evaporation over the course of an extended test, which is represented as a normalization function $N(t)$ that is defined in an appendix of the work of Becker et al. [5]. While this result, obtained via an asymptotic expansion for small amplitudes, does not exactly approximate the highly-deformed, aspherical droplets discussed in this thesis, its representation of several major features of the real droplets which deviate from the ideal case is noteworthy.

Other equations, for the surface tension and viscosity of a spherical, relatively inviscid droplet in oscillatory mode l, are given below:

$$\sigma = \frac{3\pi\rho V {f_0}^2}{l(l-1)(l+2)} \tag{4}$$

$$\mu = \frac{\tau\rho R^2}{(l-1)(2l+1)} \tag{5}$$

Equation 4 is simply Equation 1 generalized to all oscillatory modes, as derived by Rayleigh [1], and equation 5 for viscosity was derived by Lamb [6]. The marginal maximum value of suitability of these equations to a fluid system is offered as Ohnesorge number $Oh = 0.1$ by Prosperetti [7]. The Ohnesorge number is defined as

$$Oh = \frac{\mu}{\sqrt{\rho\sigma l}} = \frac{\sqrt{We}}{Re} \tag{6}$$

The formulation of Oh utilizing the Weber and Reynolds numbers gives insight into its nature as a relationship between viscous, inertial and surface tension forces. The Weber and Reynolds numbers are defined as such:

$$We = \frac{\rho u^2 l}{\sigma} \tag{7}$$

$$Re = \frac{\rho u l}{\mu} \tag{8}$$

Note that in these three dimensionless groups, l refers to the scale length of the scenario, which for a spherical droplet would be its diameter, and u refers to the velocity of the internal flow of the droplet. In particular, Equation 4 relating f_0 and σ is utilized substantially in the following study as a means of estimating the natural frequency of a droplet of a given volume with known surface tension. The evident asphericity and viscosity of the droplets studied herein conspire to reduce the accuracy of this calculation, but it suffices as a preliminary approximation. The droplets' calculated Ohnesorge numbers range from 0.005 to 0.05, indicating that their viscosities are not large enough to cause significant deviations from the analytical results on their own.

Basaran noted that at moderate to large deformation amplitudes, the behavior in time of a droplet whose deformation is described in spherical harmonics is significantly different than that of a spheroidal droplet, which he ascribed to the greater surface area of the spheroidal shape [8]. His results also indicated a greater decrease in natural frequency with high deformation amplitude for a spheroidal/ellipsoidal droplet than for a harmonic droplet; this owes itself directly to the difference in surface energies. It is possible that this has a connection to the relationship observed in this study.

Oscillation of Aspherical Droplets

In microgravity or in a medium wherein the sample droplet is neutrally buoyant, its resting shape is nearly spherical. However, for essentially any liquid in air at Earth's surface, a suspending force acting in opposition to gravity will cause the sample droplet to assume an oblate shape. This has ramifications for the droplet's natural frequency. Cummings and Blackburn highlighted that for an aspherical droplet oscillating in the fundamental mode $l = 2$, the single natural frequency will split into three or five closely spaced separate frequency bands at which the droplet will resonate, these correlating to orders $m = 0,\ \pm 1$, and ± 2 [9]. Order $m = 0$ can be said in this case to correspond to symmetry representation Σ^+, with principal orientation *z* for a droplet oscillating in a prolate-oblate manner along the *z*-axis; orders $m = \pm 1$ and $m = \pm 2$ correspond to symmetry representations Π (principal orientations *xz* and *yz*) and Δ (principal orientations x^2-y^2 and *xy*). These "principal orientations" give a sense of the fluid droplet's internal motion in each mode, e.g. with oscillations of mode $m = \pm 1$ appearing as a "wobble" at approximately 45 degrees to the axis. For pressure fields where droplet axial symmetry is maintained, Cummings and Blackburn showed that three distinct fundamental frequencies, closely spaced together, would appear due to the double degeneracy of the symmetry species corresponding to $m = \pm 1$ and $m = \pm 2$. Thus, for an axisymmetric aspherical droplet, there exist natural frequencies $\omega_{\Sigma^+} = \omega_{2,0}$, $\omega_{\Pi} = \omega_{2,\pm 1}$ and $\omega_{\Delta} = \omega_{2,\pm 2}$.

Suryanarayana and Bayazitoglu additionally noted that due to the influence of acoustic forces, the $m = 0$ mode is shifted up in frequency and the $m = 1$ mode is actually closest to the Rayleigh frequency of a volumetrically equivalent sphere [10].

The incorporation of these frequencies into the assessment of the actual natural frequency of a droplet was conducted by Egry et al. [11] and is illustrated below. Egry et al. took an average of the three frequencies, weighting the Π and Δ terms doubly due to their degeneracy, and then combined this with oscillation of their droplets' centers of mass. This second step is only necessary when the motion of the droplet over the test interval is significant; it can be seen in the source text.

$$\overline{\omega_2^2} = \frac{1}{5}\left(\omega_{2,0}^2 + 2\,\omega_{2,\pm1}^2 + 2\,\omega_{2,\pm2}^2\right) \tag{9}$$

In the more general case of asymmetric droplet oscillation, this correction can be used to more accurately represent the Rayleigh frequency; it was not applied in the present study due to the intrinsic uncertainty in visually determining a droplet's natural frequency and identifying the three split modes. Application of the technique to further study may, however, be advisable, particularly if the experimental apparatus is developed such that real-time Fourier-transformed frequency data could be collected from the oscillating droplet and the split frequencies could be physically observed.

A numerically determined result obtained by Shi and Apfel in 1994 actually points to an increase in the natural frequency of an acoustically levitated droplet at small aspect ratios [12]. Shi and Apfel explained that this character owes itself to the competing effects of changing surface tension stress and of the acoustic pressure field, which both vary with shape. The data collected in this study proved to be too noisy at low deformation amplitudes to observe this behavior, which is also more prominent in microgravity than in Earth gravity due to the deformed shape a droplet in suspended equilibrium tends to assume.

Acoustic Levitation

Some discussion on acoustic levitation beyond the basic technical features of the apparatus used in this study is warranted here. The principal reasons for its employment in this study are its flexibility with respect to droplet size and its ability to levitate nonconductive materials. Both characteristics are conducive to rapidly collecting many sets of data from droplets of various volumes. An additional benefit of the acoustic levitator used in this study is the ready adjustability of a suspended droplet's oblateness. An explanation of the working theory behind acoustic levitation makes clear why this is the case.

A transducer is often described as an object which converts electricity into another physical quantity or form of energy, i.e. light, sound or mechanical vibration, or vice versa. The core of an acoustic levitator's functionality is its transducer, and the conversion is from synthesized sinusoidal electrical signals to mechanical oscillation in a rigid, prestressed aluminum pedestal above which the droplet is levitated [13]. The conversion is achieved by exposing two piezoelectric lead-zirconium-titanate (PZT) crystals to the input sinusoidal signal via a flat copper plate sandwiched between them [14]. These two PZT crystals, the plate and the pedestal above are held together by a central bolt. A diagram of the pedestal, crystals and plate is shown in Figure 1.

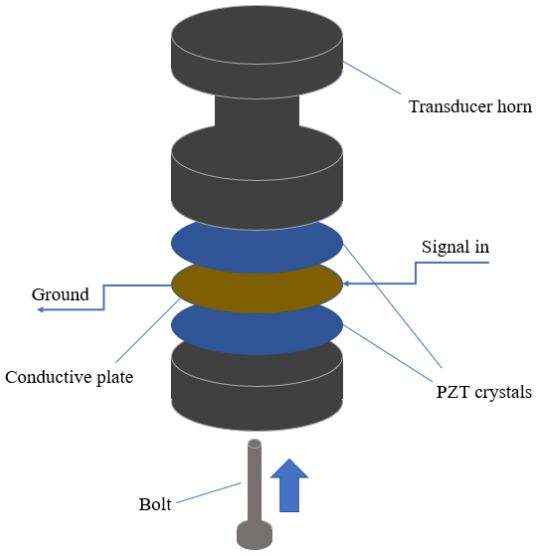

Figure 1. Acoustic levitator horn exploded view (simplified).

As described by Tian et al., the two piezoelectric crystals respond to a sinusoidal current through the plate by oscillating with opposite direction [14]. The transducer horn is constructed such that this oscillation results in a vertical displacement of the horn surface at the ultrasonic frequency input into the plate.

This ultrasonic vertical displacement creates planar pressure waves above it, so long as the surface of the transducer horn is of larger diameter than the wavelength of the sound at the levitator's resonance frequency – if this condition is not met, the shape of the pressure waves will exhibit significant curvature and degrade the levitator's effectiveness [15]. The presence of a metal reflector at a distance of an integer multiple of wavelengths from the horn causes a standing wave to develop between the two, and there are several locations in this space along the axis running through the device's center where the radiation pressure balances gravity and a droplet or other small piece of matter can be suspended in quasi-static equilibrium. Droplets suspended in this

manner were observed to occasionally translate slightly, but the restoring force of the pressure field quickly suppresses this motion.

The action of the radiation pressure in conjunction with the effect of gravity tends to force a suspended droplet into an oblate shape; with the droplet's surface area growing with increased oblateness. In the equilibrium condition, the droplet's overall surface tension force balances with the body force on the fluid inside it. It stands to reason that the radiation pressure also opposes droplet deformation in the prolate direction since a prolate deformation would force the droplet's surface to move against the pressure gradient.

Impetus for this Work: A Prior Observation

This exploration of the dependency of frequency depression rate with deformation increase on droplet size is not without precedent. In 1982, as part of an experimental study on large-amplitude free and driven oscillations of droplets, Trinh and Wang tested droplets of 0.5 and 1 cm^3 and observed that the smaller droplet's natural frequency decreased more quickly with deformation increase than the larger one [16]. Their experimental results are shown in Figure 2 (drawn directly from that paper).

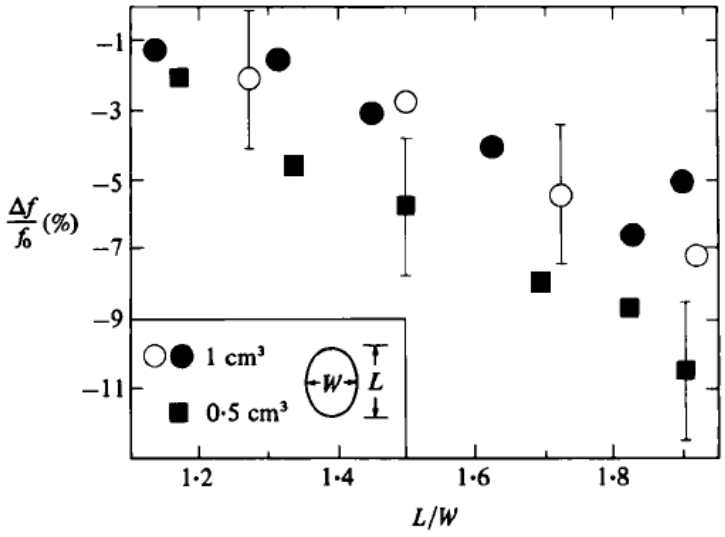

Figure 2. Data from Trinh and Wang (1982) highlighting apparent size dependency on rate of natural frequency decrease with amplitude variation.

Trinh and Wang also utilized an acoustic field to deform their droplets; however, calling it levitation would border on mischaracterization because the droplets in question did not actually require assistance to be suspended. Trinh and Wang studied the behavior of droplets of a silicone oil/carbon tetrachloride mixture in distilled water, and the droplets were nearly neutrally buoyant. They did utilize a 22 kilohertz frequency to trap the droplets in position, and so the effects of radiation pressure could not be neglected in their study; however, unlike in the case of levitating in air, the levitation pressure was not necessarily in direct opposition of gravity – this task was handled principally by the buoyant force supplied by the surrounding water. The results that Trinh and Wang obtained for the droplets suggests a size dependency, but they only studied two droplets in this phase of the battery of different experimental tests described in their paper. The intent of the study concerned in these pages is to further

explore this possible size dependency, and accounting for the myriad differences between the setup of Trinh and Wang and the acoustic levitator apparatus, droplet media and experimental technique used here is a necessary intermediate step.

Experimental Apparatus and Methodology

Apparatus Physical Description and Operating Principles

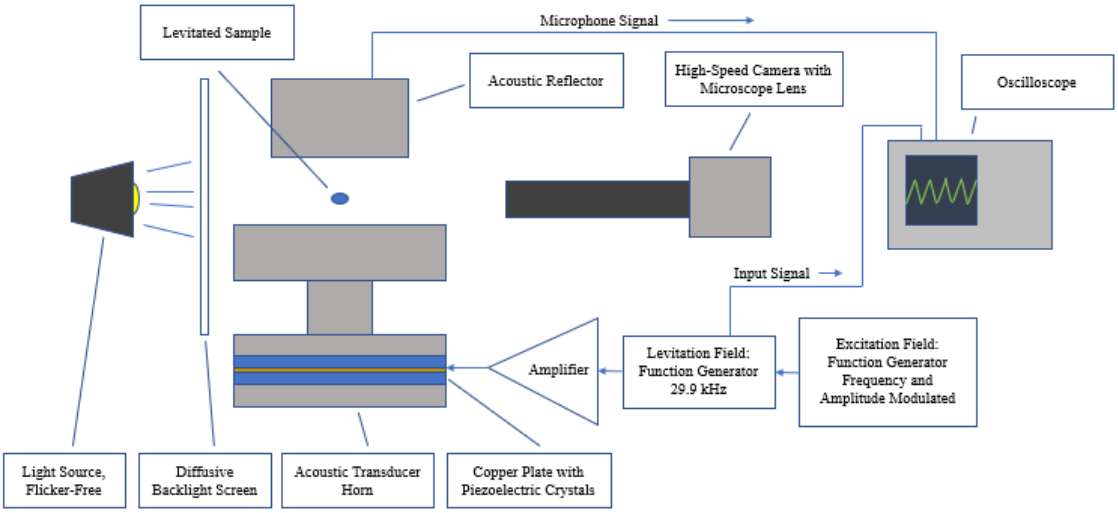

Figure 3. Schematic block diagram of acoustic levitator setup, showing signal transfer paths and apparatus major components.

The data of this study was collected utilizing an acoustic levitator on loan from Professor R. Glynn Holt at Boston University. The apparatus suspends samples by means of a standing wave pressure field between a transducer horn and a reflector [17]. Two function generators in tandem output a modulated sinusoidal signal to a copper plate between two piezoelectric crystals which convert it to a mechanical oscillation. At the resonant frequency of the apparatus (29.9 kHz in this case, slightly variable with transducer temperature), the separation between the horn and the contoured metal reflector is equal to one wavelength, thus producing approximately planar standing pressure waves between the transducer and reflector. Two nodes are created where the

gravitational interaction is balanced by pressure force; in this study, the lower one is utilized. The approximate locations of these nodes are shown in Figure 4.

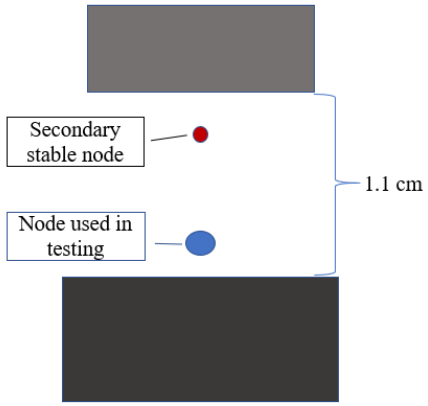

Figure 4. Schematic highlighting approximate locations of stable nodes in acoustic pressure field.

The modulation of the input by the second function generator allows for superposition of a second signal, of much lower frequency than the levitation signal, which is used to excite the droplet being examined to oscillate near its damped natural frequency.

The levitator apparatus was operated in a four-sided clear polycarbonate enclosure with a circular aperture of 70mm diameter at the front for the lens of a high-speed camera and another of 25mm next to the first for injection of the droplet into the levitation field. This enclosure served to isolate the air inside the box from eddies and air currents in the lab, which if not obstructed disturb any levitated droplet and interfere with data acquisition. Diffuse, steady backlighting of the analyzed droplets was achieved by integrating a white paper screen into the rear surface of the enclosure and training a photographic spotlight behind it so that the illuminated area of the diffuser screen was in line with the camera's field of view. A purportedly flicker-free LED bulb

was used in the spotlight; however, at the very high framerate of the video footage, some mild high-frequency flickering was still observed. This did not impact the results of the image-processing program.

Imaging and Sensing Hardware

To record high-speed video of the oscillating droplets, a Photron Fastcam Mini AX200 high-speed camera with an Infinity K2 long-range microscope lens was used. This is shown in Figure 5.

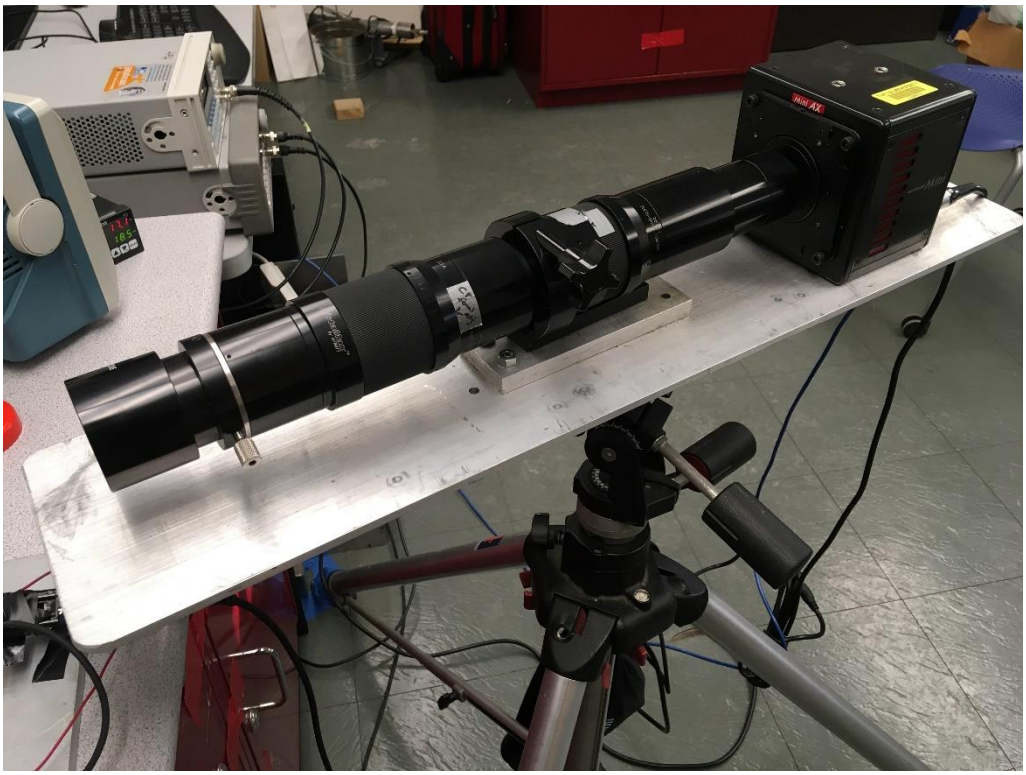

Figure 5. Photron Fastcam Mini AX200, Infinity K2 long-distance microscope lens, mount and tripod used in data collection.

The mounting baseplate supporting the camera and lens was fabricated by the author and protects the threaded interface between the two from loading stresses and jostling. Video was taken at 27,000 frames per second with a resolution of 384 by 384 pixels. The ambient temperature inside the levitator apparatus enclosure was measured using a type K thermocouple with a Minco CT16 temperature controller, which was calibrated against freezing (0°C) and boiling (100°C) water to recover an uncertainty in temperature measurement of +/- 0.3°C. This controller was kept continuously powered over the course of several days of taking data to eliminate transient sensor drift effects commonly observed on readout power-on. The thermocouple junction was placed inside the enclosure, near the transducer horn but well clear of the acoustic field.

Dimensional Calibration

In order to collect data, the high-speed camera was trained and focused on the region of interest in the transducer gap. Before a droplet was deployed, a cylindrical aluminum rod held horizontally by a free-standing fixture was inserted into the region of interest perpendicular to the camera's line of sight as shown in Figures 6 and 7. This rod was measured to be 3.18 +/- 0.01 mm in diameter, and when placed such that it passed through the levitator's stable node, it could be used in conjunction with the functionality of the camera's computer interface to set the size of its field of view and thereby calibrate dimensional measurement of the imaged samples. A grid of unit size based on this measurement was superimposed over the live image to facilitate determination of droplet dimensions *in situ*. The fineness of this grid – 0.1mm – was selected for being small enough that visually judging the droplet's dimensions to within

+/- 0.02mm was possible but large enough that the grid cells could be quickly counted to determine the droplet's observed height and width.

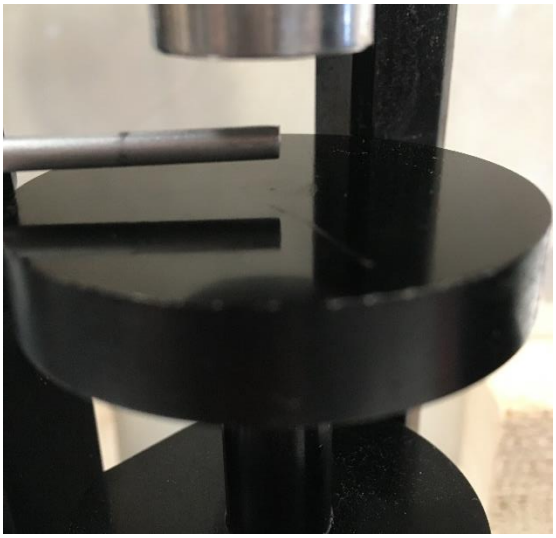

Figure 6. Detail of calibrator rod in camera field of view.

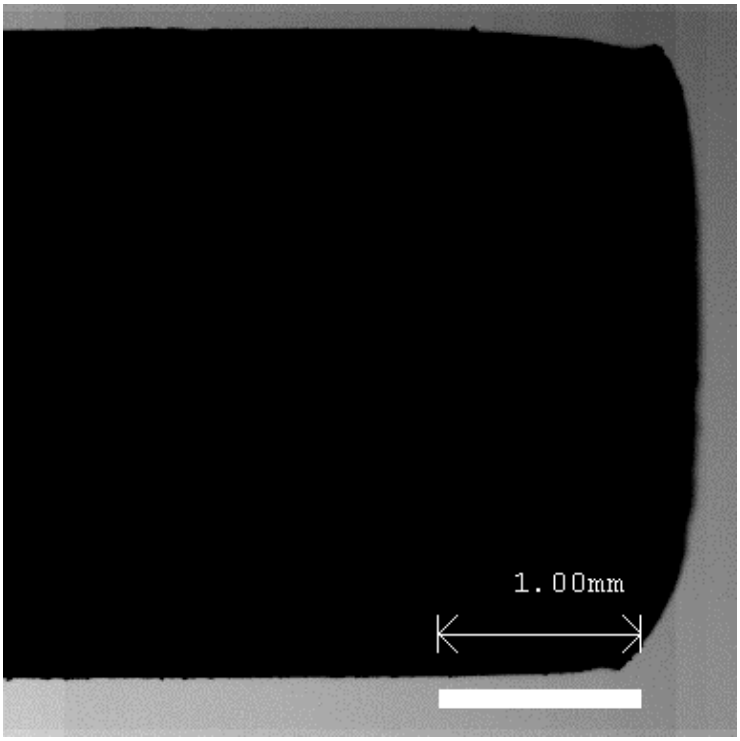

Figure 7. Screen capture of calibrator rod, with calibrated 1mm length shown.

As is evident in Figure 7, the calibrator rod is not cylindrical all the way to its end but necks down slightly due to shear stresses in the cutting process. Thus, the vertical distance between the rod's upper and lower edges near the left of Figure 7 was chosen as the calibration length, where the above-stated value and uncertainty for diameter were physically measured with a digital Vernier caliper.

Droplet Mixture Preparation

The liquid used in this study was a mixture of water and ethylene glycol at a volumetric ratio of 1:1. Equivalent volumes of each substance were drawn using syringes with volume graduations, transferred to a clean, dry beaker and thoroughly mixed. This mixture was then drawn into a third syringe with a thin, blunt-tipped hypodermic needle, where it has effectively no free surface area and thus a negligibly small rate of constituent mole fractional change due to evaporation. Volumetric uncertainty in this mixing method was determined to be approximately +/- 3%.

The constituents of water and ethylene glycol were chosen for their miscibility, relative safety to handle and availability. At 25°C, their properties are as shown in Table I.

Table I. Relevant thermophysical properties, water and ethylene glycol, 25°C

Material	Density (kg/m^3)	Viscosity (mPa s)	Surface Tension (mN/m)
Water	997	0.89	72.0
Ethylene Glycol	1110	16.1	48.0

Binary liquid mixture surface tension and viscosity measurements are a subject of much research. However, for the purposes of this study, surface tension is the only quantity necessary to be known with much precision.

Mixture density is the product of a simple calculation:

$$\rho_{mix} = v_{water}\rho_{water} + v_{EtG}\rho_{EtG} \tag{10}$$

In this equation, v_{water} and v_{EtG} are the volume fractions of each constituent. Since this is a binary mixture, $v_{water} = 1 - v_{\mathrm{EtG}}$ and the mixture density can be easily solved for, as the constituent density values are known to very high precision.

Mixture viscosity is not such a trivial relationship; several foregoing examples of hypotheses for the relationships between constituent viscosities and mixture viscosities are discussed by van der Wyk [18]. It was observed that none of the classical equations, in the form

$$f(\mu_{mix}) = g(c_1)f(\mu_1) + g(c_2)f(\mu_2) \tag{11}$$

provided results that compared well to empirical data in all cases; errors of up to 20 percent were observed when mixing materials of very different physical constants. However, for the purposes of this work, uncertainties of this order in the value of mixture viscosity did not greatly impact the results. An approximate value for mixture viscosity was necessary in order to determine what volume fraction of ethylene glycol should be used in the mixture. A relatively narrow range of viscosities ultimately proved suitable for testing.

To digress in the name of explaining the presence of bounds on droplet liquid viscosity, it was observed that levitating and attempting to excite droplets of pure water using the acoustic levitator resulted in unpredictable oscillations. Higher-order modes

(principally $l = 2, m = 1$) were observed which make determination of the characteristics of the $l = 2, m = 0$ mode very difficult. It has been shown that oscillatory modes beyond the fundamental oblate-prolate mode decay significantly more quickly than it [5]. The relatively small amplitudes of these oscillations in tandem with their higher viscosity-governed decay rates mean that with a relatively viscous liquid, oscillations can be excited which appear to have no higher-order character. Conversely, oscillating water results in higher-order oscillations of significant amplitudes and attendant noise in collected data. Only a relatively small adjustment in total viscosity proved necessary to mitigate this issue, however.

The upper bound in viscosity stemmed from the need to observe several oscillatory periods within the transient free-decay interval in order to document the change in period lengths. As explained earlier, the time constant τ_l governing the exponential rate of decay of oscillation amplitudes may be related to the viscosity of the medium by Equation 2. At the relatively low viscosities examined in this study, the damped natural frequency is dependent only on droplet surface tension and mass, and so if τ_l were on the order of the oscillatory period, only one or two peaks would be observed in the transient window before the oscillation is entirely damped out. Thus, an effective viscosity ceiling was imposed by the experimental need to acquire useful data.

This bounding of the viscosities led to the author utilizing one of the simple additive viscosity formulas described by van der Wyk [18] to determine approximate viscosities of various mixtures of water and ethylene glycol. The formula chosen was proposed by Arrhenius in 1879, and is transcribed in Equation 12 [19].

$$ln\,\mu_{mix} = x_{EtG}\,ln\,\mu_{EtG} + x_{water}\,ln\,\mu_{water} \quad (12)$$

This survey concluded with the author settling on an aqueous mixture with 50 percent ethylene glycol by volume, which has a viscosity of approximately 3 mPa s.

Mixture surface tension is also a nonlinear relationship, and the treatment used herein stems from the results of Equation 13, originally developed by Connors and Wright in 1989 [20].

$$\sigma_{mix} = \sigma_2 - \left(1 + \frac{\alpha x_2}{1 - \beta x_2}\right) x_1(\sigma_2 - \sigma_1) \quad (13)$$

The coefficients α and β were experimentally determined by Tsierkezos and Molinou for the system of ethylene glycol and water, with the former being subscript 1 and the latter being subscript 2 in the above more general equation [21]. Tsierkezos and Molinou evaluated the coefficients at increments of 10°C, and to accurately determine them at the range of temperatures normally encountered in the laboratory (20 - 30°C), the author linearly interpolated between the data points determined by Tsierkezos and Molinou. The obtained results were cross-checked against experimental data by Nakanishi et al. and found to be in good agreement [22]. Further linear interpolation to determine accurate values for constituent surface tensions at variable temperatures was enabled by a database of pure liquid surface tensions generated by Jasper [23]. The coefficients and values used are given for reference in Table II.

Table II. Constituent Surface Tensions and α and β Coefficients

Quantity	Value, 20°C	Value, 30°C	Value, 40°C	Source
σ_{water}	71.72 mN/m	70.08 mN/m	68.38 mN/m	[23]
σ_{EtG}	48.43 mN/m	~	46.65 mN/m	[23]
α	0.6912	0.7253	0.7623	[21]
β	0.8810	0.8859	0.8800	[21]

Data also exist to generalize this method for a larger range of mixture temperatures; these can be found in their respective source texts.

Accounting for Evaporation

One complication with using water and ethylene glycol arises in observing their very different vapor pressures at room temperature and typical relative humidity levels. Water has a vapor pressure of approximately 3.17 kPa at 25°C while ethylene glycol's value at the same temperature is 0.012 kPa. This is indicative of a much higher rate of evaporation for water (a factor of at least two orders of magnitude for a given surface area), which is the basis of an assumption made by the author at this point in the analysis that water is the only species evaporating from levitated droplets over the duration of evaluation. This assumption is borne out experimentally in work by Rusdi et al. [24]. A droplet's dimensions were measured immediately after introduction into the field and then immediately after an evaluation interval, the volume at each point was calculated and the change in volume was assumed to be entirely due to evaporating water. With an initial ethylene glycol volume fraction of 0.5, the final volume fraction (and thus mole fraction, which is needed for the surface tension calculation) could be computed.

Data Acquisition

The levitation signal was initially set with the output of the modulating function generator (which supplies the excitation frequency) turned off. The input signal was adjusted until the microphone within the acoustic reflector indicated that the apparatus

was oscillating at resonance frequency. A sample droplet was introduced to the field using a syringe and hypodermic needle and any present translational motion due to droplet elastic rebound off the needle after insertion was permitted to die away. The amplitude of the levitation frequency was typically reduced slightly, as high levitation drive provides greater force to overcome the droplet's adhesion to the needle tip but also forces it into a more oblate shape. This reduction was conducted keeping in mind that for this apparatus the oscillation frequency is imparted as a modulation of the levitation frequency and is therefore contingent on the latter having adequate amplitude. The live feed from the camera was paused, and the calibrated unit-size grid was used to manually determine the droplet major and minor axis diameters as illustrated in Figure 8.

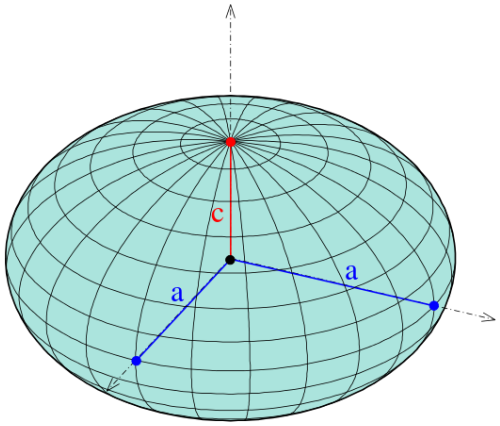

Figure 8. Oblate spheroid diagram with characteristic dimensions highlighted.

The ambient temperature near the region of interest was measured, it and the sample's composition were used to determine surface tension, and this value and the sample's physical dimensions were input into Rayleigh's equation for the fundamental oscillatory mode $l = 2$, reiterated from earlier and here shown [1].

$$f_0 = \sqrt{\frac{8\sigma}{3\pi\rho V}} \quad (1)$$

For this relation to be exactly true, the droplet must be spherical and the oscillations very small. The confluence of gravitational force and acoustic pressure precludes satisfaction of the first condition, and this study's goal of examining large oscillations precludes satisfaction of the second, but as a preliminary estimate this equation has some utility. The excitation signal output was initiated at the frequency indicated by Equation 1 and then the frequency modulated until the resonant frequency was found by observation. This step necessitated use of the K2 long-range microscope lens. Once resonance was found, the camera was set to record and the excitation frequency abruptly cut, resulting in recording of an exponential decay of droplet oscillations which was saved for processing. This decay's amplitude as a function of time may be approximated by Equation 2 for a surface oscillation of mode l (reiterated from above).

$$A_l(t) = A_{0l}e^{\frac{-t}{\tau_l}} \quad (2)$$

The time constant τ_l is a viscosity-dependent parameter which may be determined for a free-decay oscillating system by fitting an exponential curve to the oscillation between when the oscillation drive is removed and when the amplitude becomes on the order of signal noise. This study concerns itself with mode $l = 2$, with effort taken to obtain data exhibiting this mode in isolation from others.

Parameterization of Deformation

The droplet's deformation as a function of time is observed as both change in height and change in width. If the droplet's volume undergoes no significant change

over the course of an oscillatory period, height and width deformation about the droplet's resting dimensions are coupled together and can both be defined by one quantity, hereafter called δ, which is normalized against a droplet's resting dimensions so droplets of different sizes can be directly compared. Figure 9 illustrates how a droplet's height and width relate to δ when the oscillation is symmetric about the vertical axis.

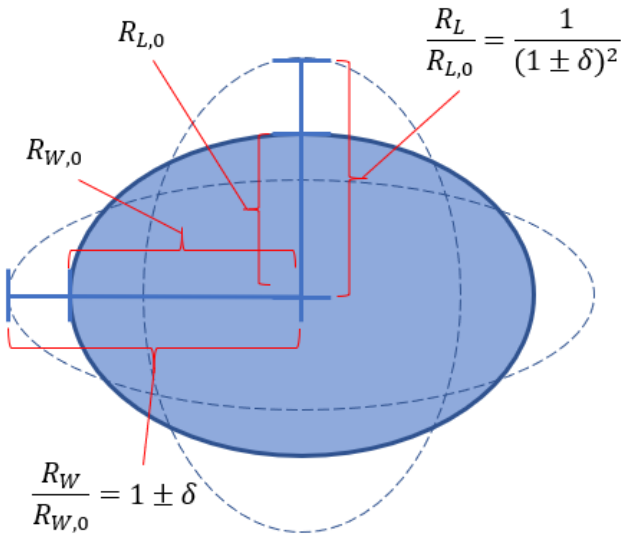

Figure 9. Definition of δ in terms of droplet width and height as a function of time.

Here, $R_{L,0}$ and $R_{W,0}$ are the resting half-height and half-width, respectively, and R_L and R_W vary in time. These quantities normalized against the resting values may be expressed in terms of δ by the expressions shown above. Practically, this means that as δ increases, the instantaneous width of the droplet increases, and the height decreases at a faster rate. This obeys volume constancy because the (assumed) axially symmetric droplet's width out of this page also increases. The resting deformation of the droplet from the sphere with radius R_0 may be described as δ_0, as in Figure 10.

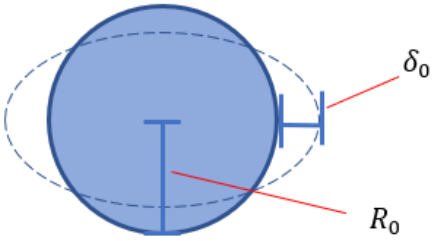

Figure 10. Definition of the resting deformation δ_0 due to the balance of gravity and acoustic radiation pressure.

Incorporating the total time-variant deformation from the spherical shape Δ, the deformation from the elliptical resting shape is written as

$$\delta = \Delta - \delta_0 \tag{14}$$

Thus, δ accurately describes the mode $l = 2$ oscillatory deformation if the ellipsoid assumption holds. In Figure 11, a comparison between δ, height and width as a function of time for a representative droplet illustrates their relationship.

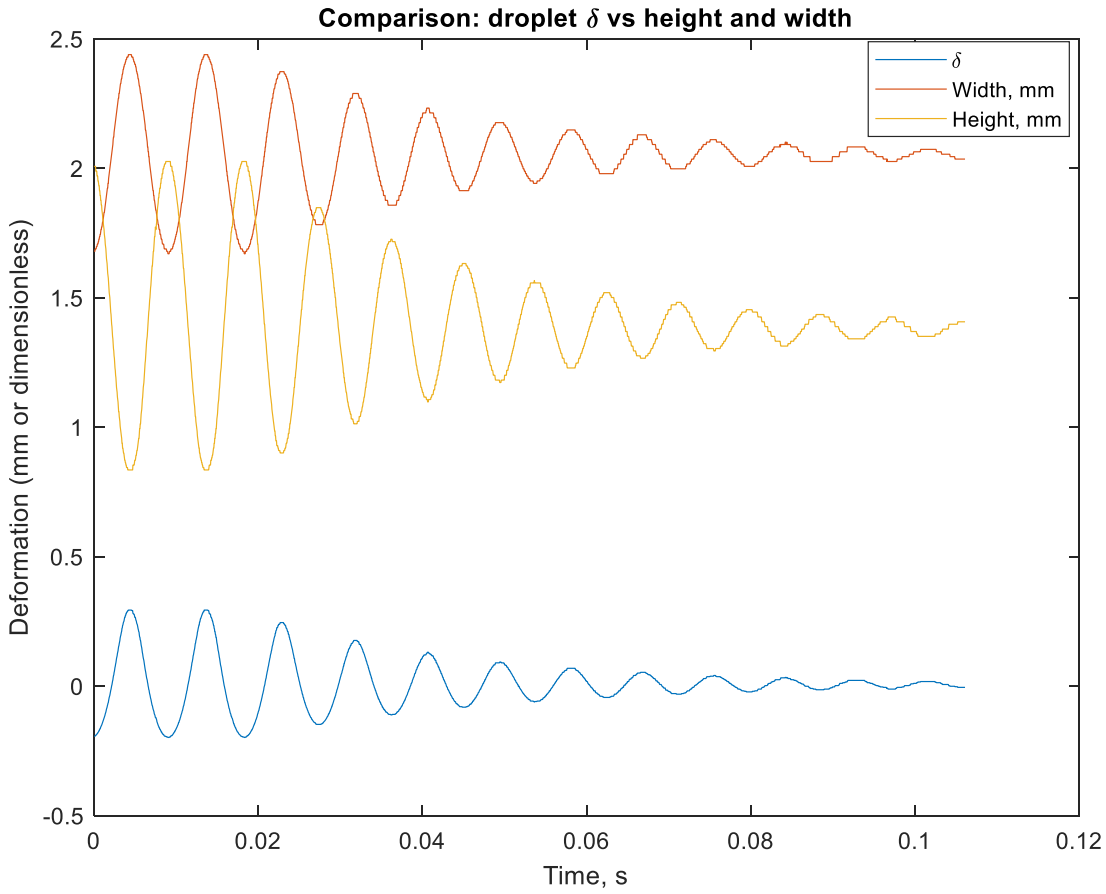

Figure 11. Different representations of droplet deformation in time: δ, width and height.

The direct proportional relationship between δ and width is evident, while the inverse-square relationship between δ and height can also be seen.

Data Processing

Each frame of the video file was read into a MATLAB program (included in appendix) which converted it into a binary array and removed the transparency artifact in the middle of the droplet as shown in Figure 12.

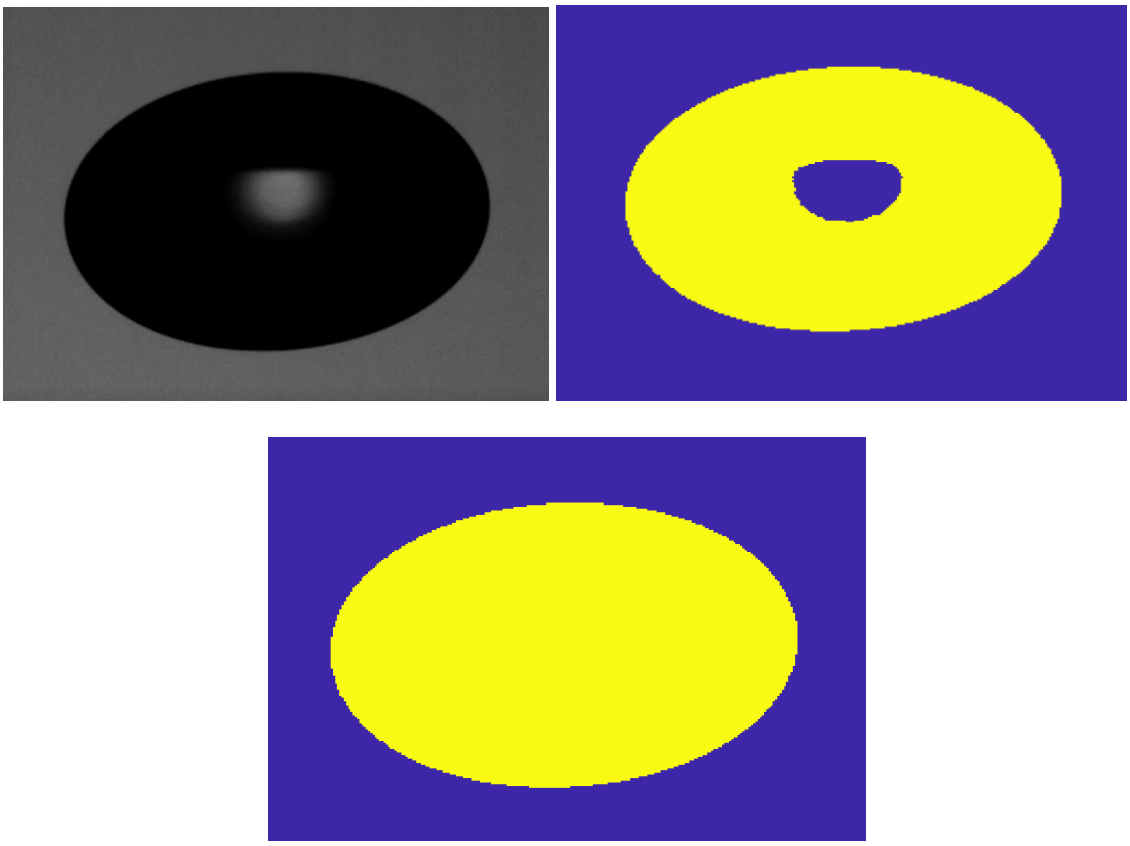

Figure 12. Three stages of video frame-by-frame processing to measure droplet width and height.

The pixels within the droplet's bounds in the horizontal and vertical directions were counted, and the resultant width and height values were converted to millimeters using the calibrated camera field-of-view dimensions. Peaks in the time-domain signal and the number of frames between each were identified as shown in Figure 13, and the camera frame rate was incorporated to yield frequency data in hertz.

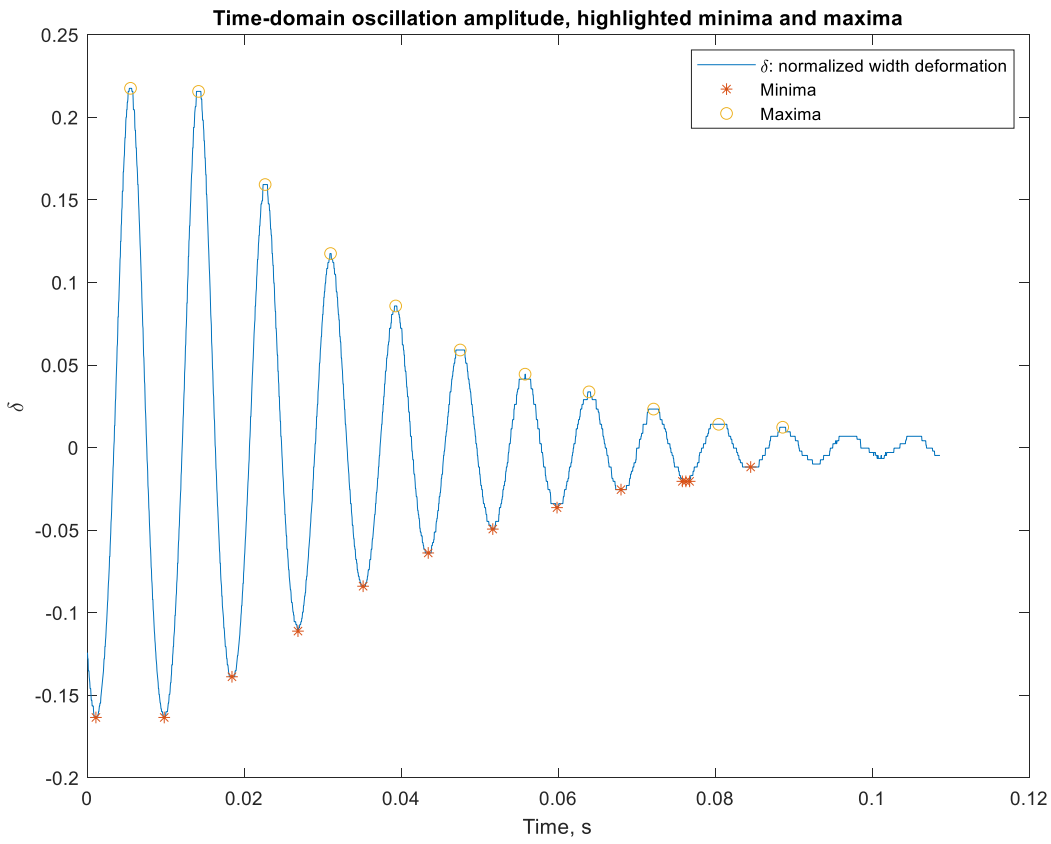

Figure 13. Time-domain δ data with maxima and minima indicated.

An alternative method of measuring the time-varying period within the window of transient behavior consists of measuring the zeros of the time-domain δ data and isolating the half-periods corresponding to the oblate and prolate phases of the oscillation. This half-period data can then be multiplied by two, and the reciprocal of this quantity can be taken to determine a representative frequency for a given oscillation. This method exposes the difference in time the droplet spends in the oblate versus the prolate phases of oscillation as illustrated by Foote as well as Tsamopoulos and Brown [2], [4]. The points under consideration are shown in Figure 14.

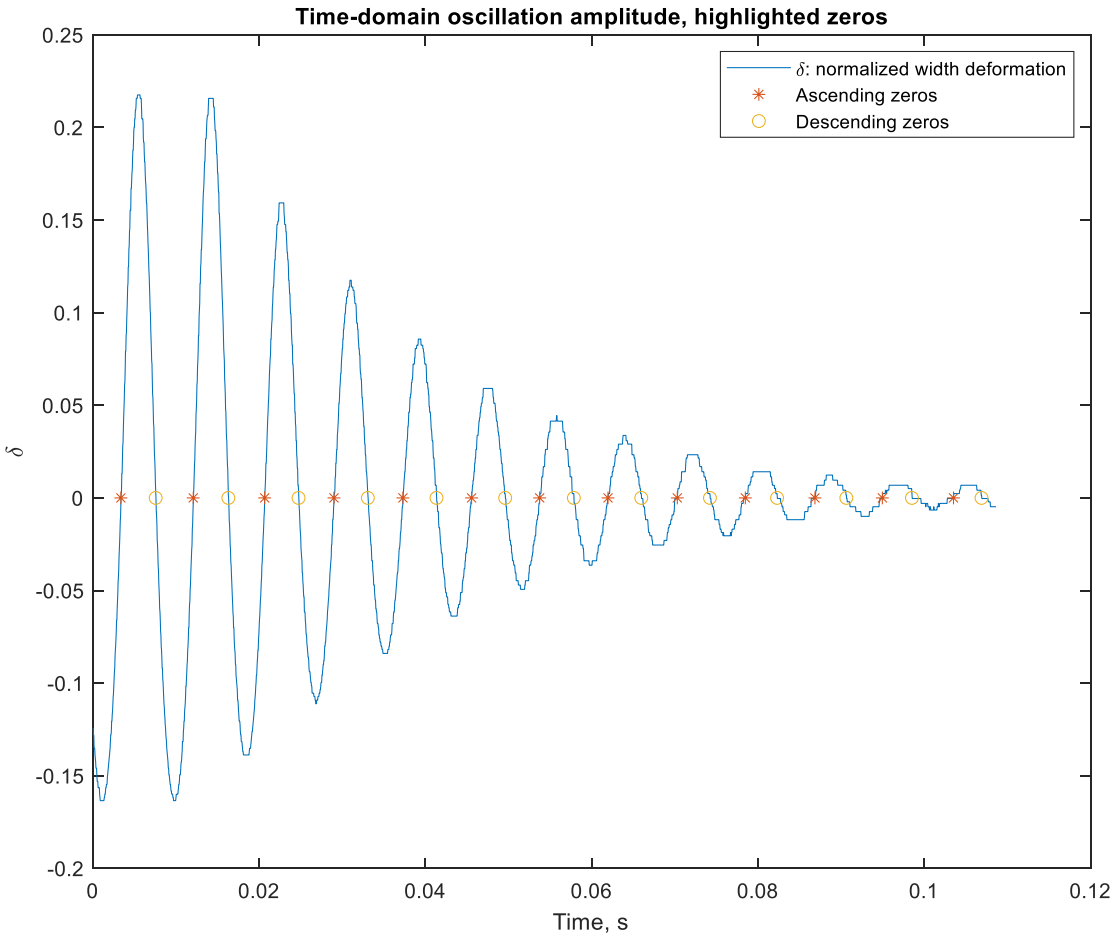

Figure 14. Time-domain δ data with ascending and descending zeros indicated.

A relationship between oscillatory frequency and droplet deformation can thus be determined via either method. The deformation is normalized against the resting dimensions of the droplet, and the observed frequencies are normalized against the theoretical Rayleigh natural frequency of a spheroid of equivalent volume to the droplet under consideration.

The received height data displays significant discretization, particularly at small deformations; very closely spaced double peaks such as the tenth minimum in Figure

13 can result. Correction of this via moving-mean methods or other smoothing could produce an incorrectly located resultant peak, so this data point was not used in further analysis.

Investigation into similar studies of oscillating droplet transient-behavior observation for determining surface tension and viscosity uncovers the use of more sophisticated means of measuring droplet deformation via image processing. Kremer et al. utilized a Canny edge-detection algorithm and curve-fitting to either side of a droplet about which a principal-axis transformation was performed to account for tilting in the field to recover droplet volume [25], which avoids many of the assumptions made in the current study.

Data Reduction

The method of finding the high-deformation natural frequency of studied droplets – a ballpark estimate using Rayleigh's formula (Equation 1) followed by visual observation of the droplet's deformation amplitude for a range of frequencies near that estimated value at a given oscillation drive voltage – leaves significant room for error. In particular, the droplet asphericity means that what would have been observed with suitable equipment would have been three natural frequencies, closely spaced together; visually, this is observed as a relatively broad frequency band over which the droplet deformation amplitude seemed not to change significantly but was clearly higher than at frequencies outside this resonance "plateau". The uncertainty here means that the high-deformation natural frequency was often significantly undershot (broadly

speaking, by 6 Hz or more). This results in behavior that deviates from that of a droplet with smaller error even if they are approximately the same size, as shown in Figure 15.

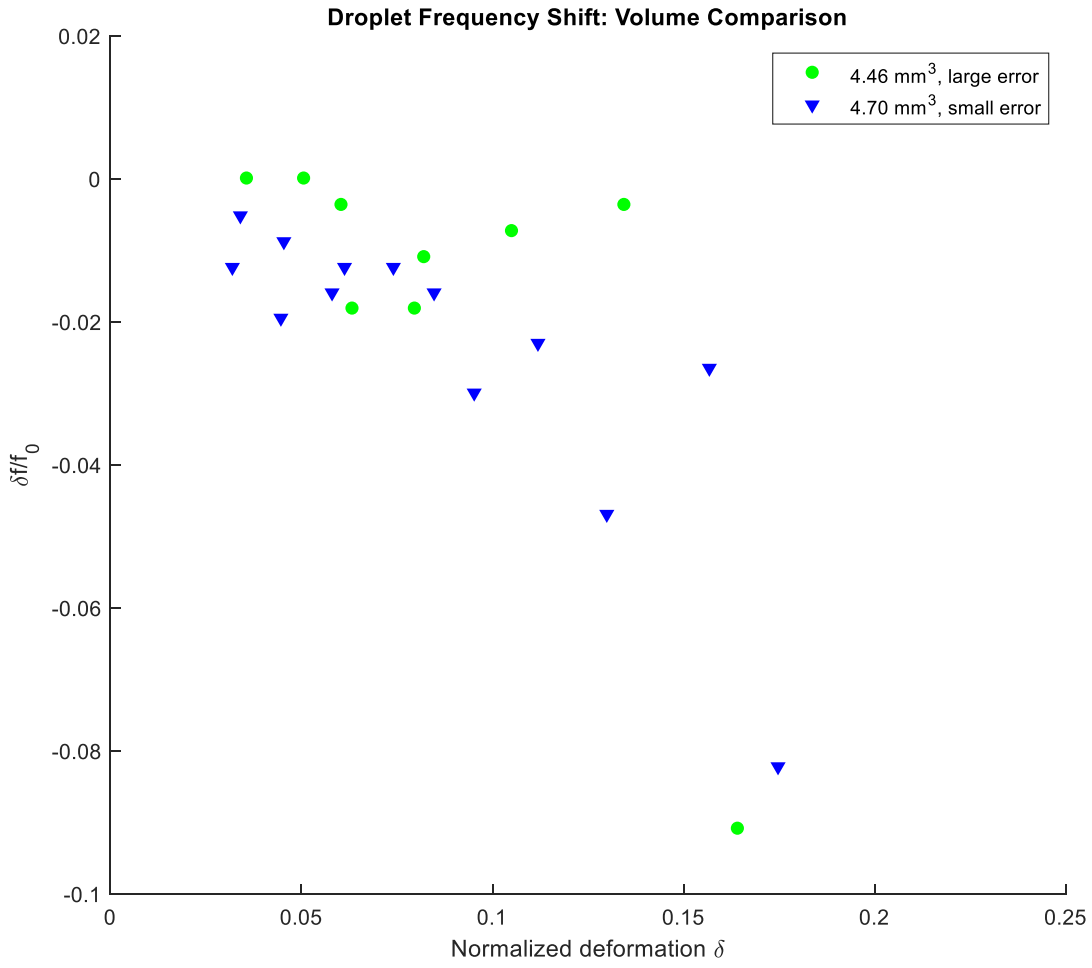

Figure 15. Illustration of data with large and small errors in driven frequency vs. high-deformation free-decay natural frequency.

The 4.46 mm^3 droplet sees a spike in frequency immediately after the oscillation drive is removed which is not present in the behavior of the 4.70 mm^3 droplet. It correspondingly was driven at a frequency much lower than its apparent high-deformation natural frequency, whereas the 4.70 mm^3 droplet's natural frequency was

guessed more accurately. Discrimination of data was conducted on this basis, with droplets with large errors between driven and free-decay high-deformation natural frequencies not considered in the following analysis.

Kremer et al. and Langstaff et al., who measured surface tension and viscosity with the oscillating-droplet method via acoustic and aerodynamic levitation respectively, observed a difference between the driven and free-decay natural frequencies of observed droplets; when the oscillation drive is removed, both parties noted a near-instant adjustment to the unforced natural frequency [25], [26]. To observe this result with certainty in this study, frequency-amplitude measurements would have been necessarily taken in real time; however, this behavior may be present in Figure 15 where an inaccurate guess of free-decay frequency is made, and the droplet's oscillation appears to initially overshoot even its low-deformation natural frequency. This could also be indicative of the initial presence and then damping-out of a higher-order oscillatory mode.

Results

Definition of Data Point Quantities

The data collected with the use of the acoustic levitator apparatus and high-speed camera footage consists of height and width deviations from a given droplet's resting dimensions coupled with points in time where peaks (maxima and minima) of each quantity are observed. The time differences between peaks were computed within the transient-behavior window, and the reciprocal of each resultant value was taken to generate a set of peak-to-peak frequency data points for each dataset. The theoretical Rayleigh natural frequency for each droplet was calculated using its volume, obtained via measuring height and width in the resting state and making the well-considered assumption that the droplet is ellipsoidal when at rest. The obtained frequency values as a function of time for each dataset are normalized against the Rayleigh frequency, and 1 is subtracted from the quotient in order to obtain a derived quantity that represents error in frequency relative to the zero-amplitude natural frequency. This is displayed in Figures 16 and 17 on the ordinate axis.

The data on the abscissa axis represent the deformation of the droplet from its resting shape. This is parameterized as δ, by which both the droplet vertical and horizontal deformations can be quantified, again assuming that the droplet is ellipsoidal. In Figures 16 and 17, filled-in data points represent δ minima and open points represent maxima.

Plots of Selected Data, Peak-to-Peak Period Measurement

A survey of droplets which represent a range of volumes at very similar aspect ratios (defined hereafter as height divided by width) is shown in Figure 16. The shown droplets all have aspect ratios of between 0.672 and 0.682.

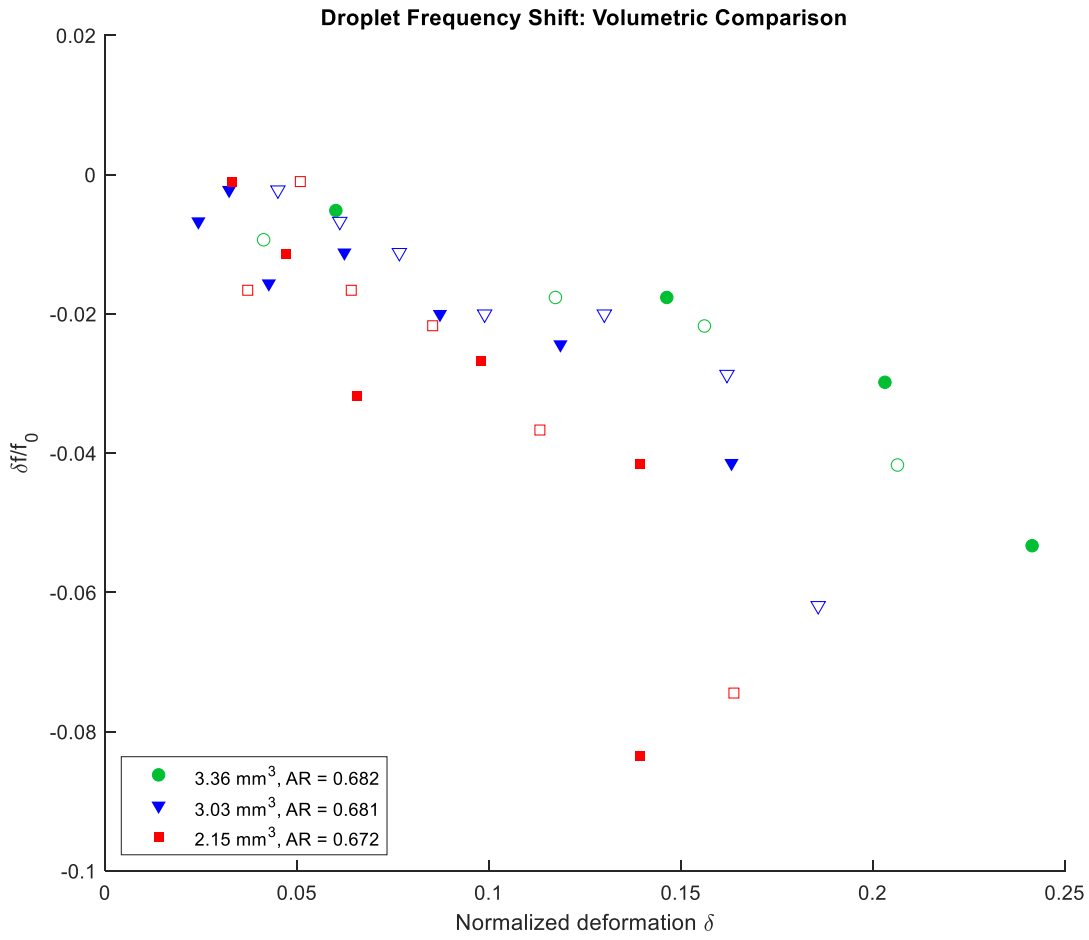

Figure 16. Normalized frequency shift vs. δ for droplets of different volumes and similar aspect ratios.

Figure 17 shows a survey of droplets with similar volumes and a range of aspect ratios between 0.637 and 0.704. All represented droplets fall between volumes of 3.18 and 3.7 mm^3.

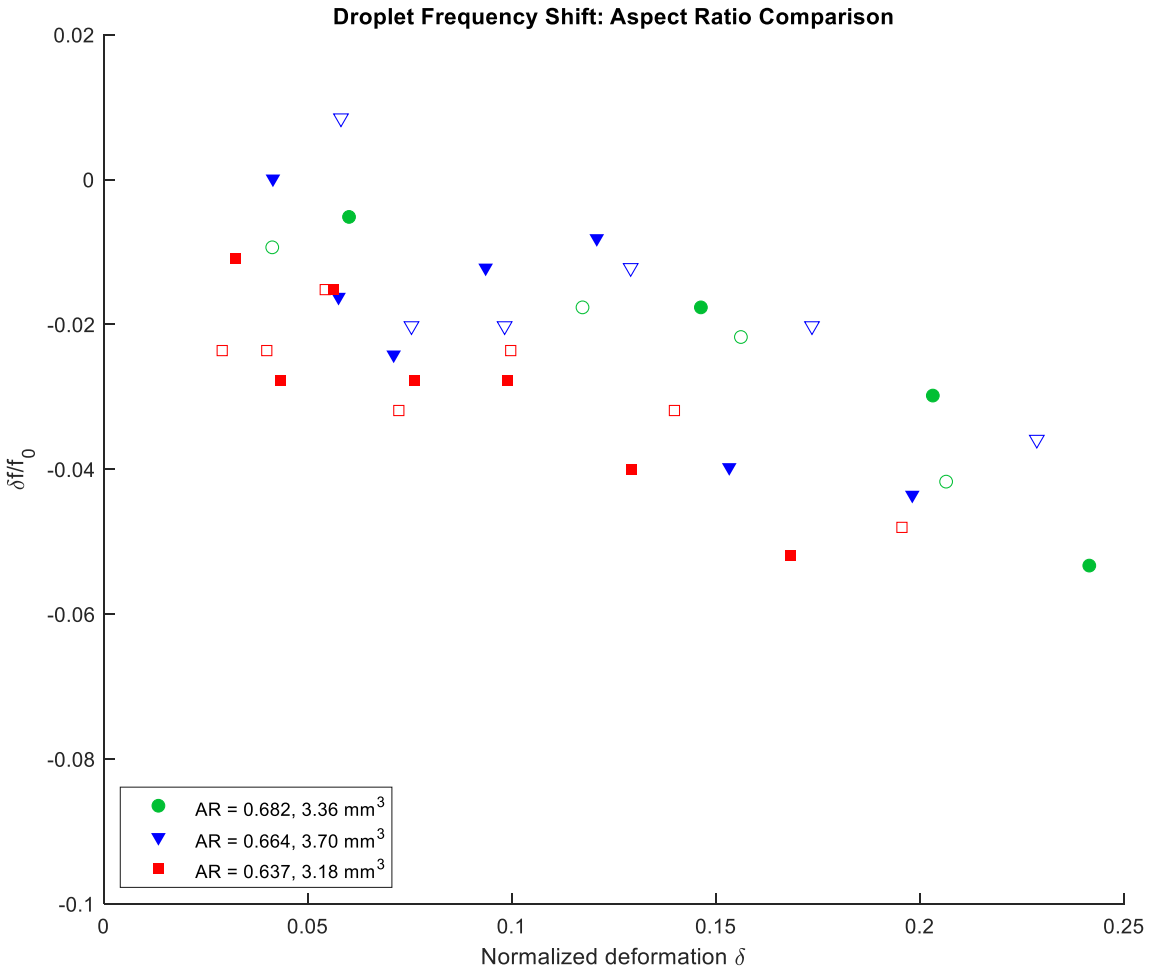

Figure 17. Normalized frequency shift vs. δ for droplets of similar volumes and different aspect ratios (height/width).

Tabulated Data Points, Peak-to-Peak Period Measurement

This section contains all the data represented in Figures 16 and 17. Five datasets are present because one droplet (3.36 mm^3, AR = 0.682) was determined suitable for both comparisons.

Table III. 3.36 mm^3, Aspect Ratio 0.682

Maxima		Minima	
$\delta f/f_0$	δ	$\delta f/f_0$	δ
-0.06087	0.206374	-0.06087	0.241447
-0.0417	0.206374	-0.0533	0.241447
-0.02174	0.156092	-0.02982	0.203112
-0.01765	0.117288	-0.01765	0.146287
-0.00936	0.041271	-0.00516	0.060084
-0.06087	0.206374	-0.06087	0.241447

Table IV. 3.03 mm^3, Aspect Ratio 0.681

Maxima		Minima	
$\delta f/f_0$	δ	$\delta f/f_0$	δ
-0.06986	0.185725	-0.06191	0.163146
-0.06191	0.185725	-0.04143	0.163146
-0.02871	0.161966	-0.02439	0.118584
-0.02003	0.130019	-0.02003	0.087202
-0.02003	0.098847	-0.01121	0.062315
-0.01121	0.076628	-0.01564	0.042628
-0.00673	0.061113	-0.00222	0.032283
-0.00222	0.044993	-0.00673	0.02428

Table V. 2.15 mm^3, Aspect Ratio 0.672

Maxima		Minima	
$\delta f/f_0$	δ	$\delta f/f_0$	δ
-0.08344	0.16377	-0.08344	0.139431
-0.07445	0.16377	-0.08344	0.139431
-0.03668	0.11324	-0.04157	0.139431
-0.0217	0.085309	-0.02675	0.097973
-0.01661	0.064106	-0.03174	0.065519
-0.001	0.050838	-0.01146	0.046994
-0.01661	0.037134	-0.001	0.033029

Table VI. 3.70 mm^3, Aspect Ratio 0.664

Maxima		Minima	
$\delta f/f_0$	δ	$\delta f/f_0$	δ
-0.04332	0.294013	-0.05074	0.194607
-0.04332	0.292226	-0.02814	0.196298
-0.02036	0.230376	-0.02427	0.151454
-0.00443	0.175289	0.007858	0.118996
0.003727	0.130872	0.003727	0.091771
-0.00443	0.099991	-0.00846	0.069237
-0.00443	0.077166	-0.00037	0.055728
0.024726	0.059891	0.016222	0.039656

Table VII. 3.18 mm^3, Aspect Ratio 0.637

Maxima		Minima	
$\delta f/f_0$	δ	$\delta f/f_0$	δ
-0.06363	0.270216	-0.07124	0.199091
-0.04802	0.195548	-0.05197	0.168233
-0.03188	0.139808	-0.04002	0.129316
-0.02361	0.099698	-0.02777	0.099003
-0.03188	0.072281	-0.02777	0.07607
-0.01519	0.054252	-0.01519	0.056296
-0.02361	0.039932	-0.02777	0.043401
-0.02361	0.029011	-0.01093	0.032369

Plots of Selected Data, Zero-to-Zero Period Measurement

Figure 18 plots the deformation data for droplets of several different volumes, obtained via the zero-to-zero measurement method.

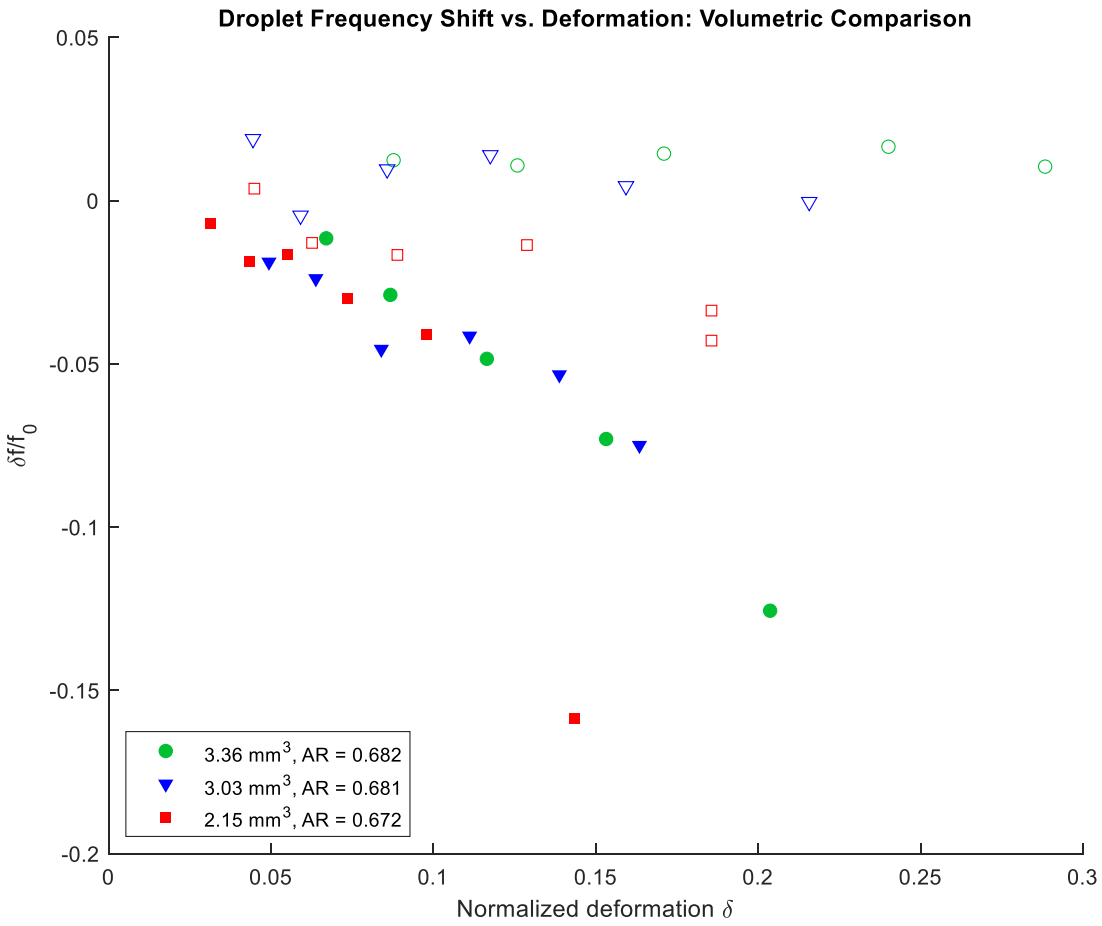

Figure 18. Normalized frequency shift vs δ for droplets of different volumes and similar aspect ratios. Values measured using zero-to-zero technique.

Figure 19 plots deformation data for droplets of a range of aspect ratios (height/width), with data points recovered using the zero-to-zero method.

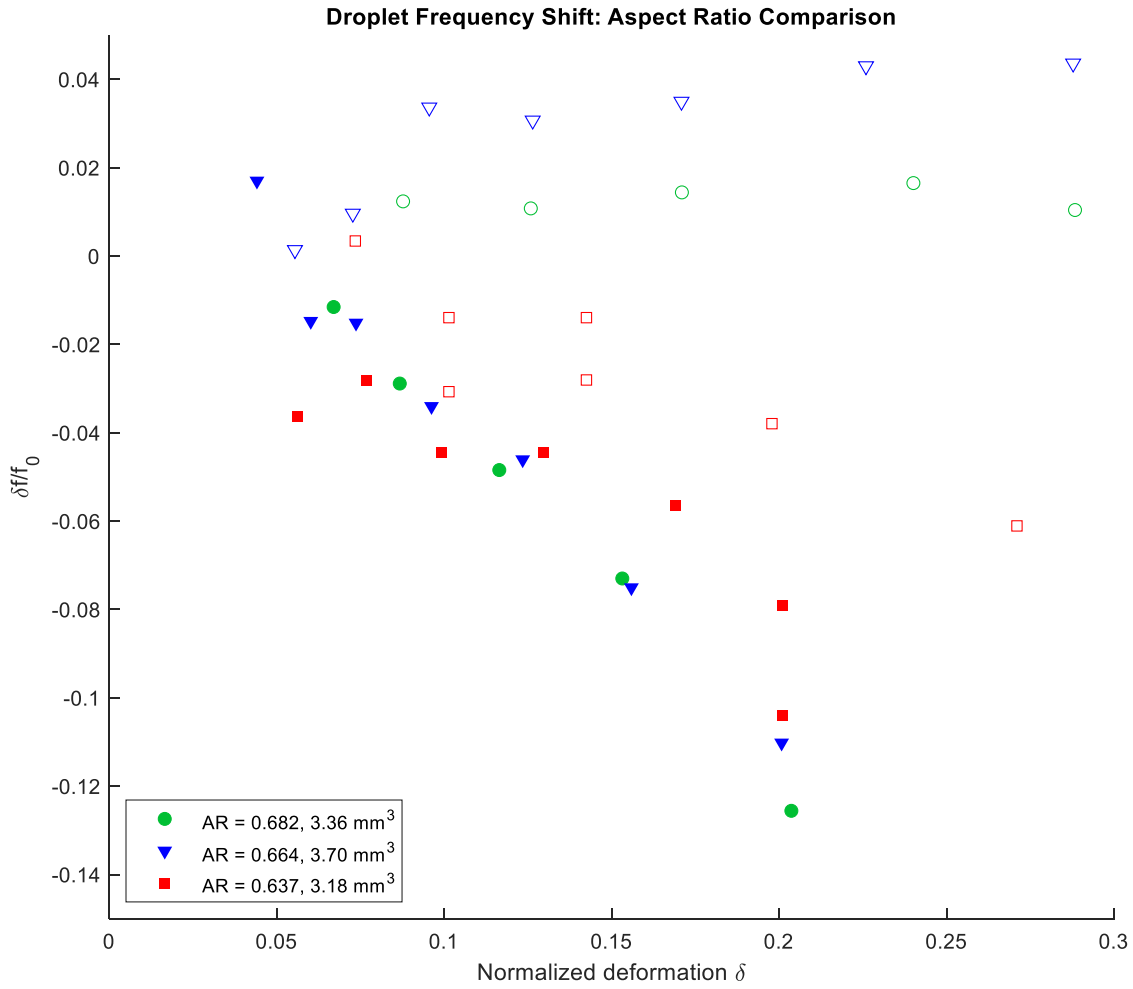

Figure 19. Normalized frequency shift vs. δ for droplets of similar volumes and different aspect ratios.

Tabulated Data Points, Zero-to-Zero Data Measurement

This section contains all the data points represented in Figures 17 and 18. As for the peak-to-peak data tables, there are only five tables because one data set (whose information is contained in Table VIII) is shown in both plots.

Table VIII. 3.36 mm^3, Aspect Ratio 0.682

Maxima		Minima	
$\delta f/f_0$	δ	$\delta f/f_0$	δ
-0.01166	0.288338	-0.10969	0.203658
0.010428	0.288338	-0.12558	0.203658
0.016524	0.240089	-0.07299	0.153183
0.014417	0.17097	-0.04844	0.116451
0.010793	0.125864	-0.02886	0.086743
0.012384	0.087731	-0.01153	0.066997

Table IX. 3.03 mm^3, Aspect Ratio 0.681

Maxima		Minima	
$\delta f/f_0$	δ	$\delta f/f_0$	δ
-0.02923	0.217568	-0.10977	0.163429
-0.00038	0.215702	-0.07493	0.163429
0.004467	0.159281	-0.05331	0.138775
0.013957	0.117519	-0.04145	0.111145
0.009617	0.085757	-0.0455	0.083959
-0.00456	0.059094	-0.02386	0.063802
0.0189	0.044454	-0.0188	0.049359
-0.02923	0.217568	-0.10977	0.163429

Table X. 2.15 mm^3, Aspect Ratio 0.672

Maxima		Minima	
$\delta f/f_0$	δ	$\delta f/f_0$	δ
0.002007	0.185611	-0.16069	0.145411
-0.04286	0.185611	-0.15872	0.143415
-0.03367	0.185611	-0.04113	0.097895
-0.01359	0.128805	-0.03002	0.073573
-0.01662	0.088907	-0.01647	0.055183
-0.01293	0.062636	-0.01848	0.043431
0.003683	0.044873	-0.00697	0.031423

Table XI. 3.70 mm^3, Aspect Ratio 0.664

Maxima		Minima	
$\delta f/f_0$	δ	$\delta f/f_0$	δ
0.00995	0.28957	-0.08225	0.19905
0.043617	0.287783	-0.11021	0.200741
0.043007	0.225932	-0.07506	0.155897
0.034972	0.170846	-0.04608	0.123439
0.030708	0.126428	-0.03403	0.096214
0.033657	0.095548	-0.01515	0.07368
0.009632	0.072723	-0.01475	0.060171
0.001386	0.055448	0.017007	0.044099

Table XII. 3.18 mm^3, Aspect Ratio 0.637

Maxima		Minima	
$\delta f/f_0$	δ	$\delta f/f_0$	δ
-0.01935	0.271003	-0.10193	0.199406
-0.06109	0.271003	-0.10393	0.200974
-0.03794	0.197862	-0.07901	0.200974
-0.02805	0.142474	-0.05636	0.16904
-0.01394	0.142474	-0.04447	0.129628
-0.01394	0.101417	-0.04447	0.099075
-0.0307	0.101417	-0.02819	0.076945
0.003414	0.073469	-0.0364	0.056174

Discussion

Interpretation of Results: Peak-to-Peak Data

Throughout the study to this point, the assumption has been made that the droplets being evaluated are ellipsoidal. The validity of this assumption was tested by plotting the characteristic radius R_0 of the sphere of equivalent volume at each frame. In accordance with the ellipsoid assumption, there would be no variation in this quantity; however, this proved not to be the case as indicated by Figure 20.

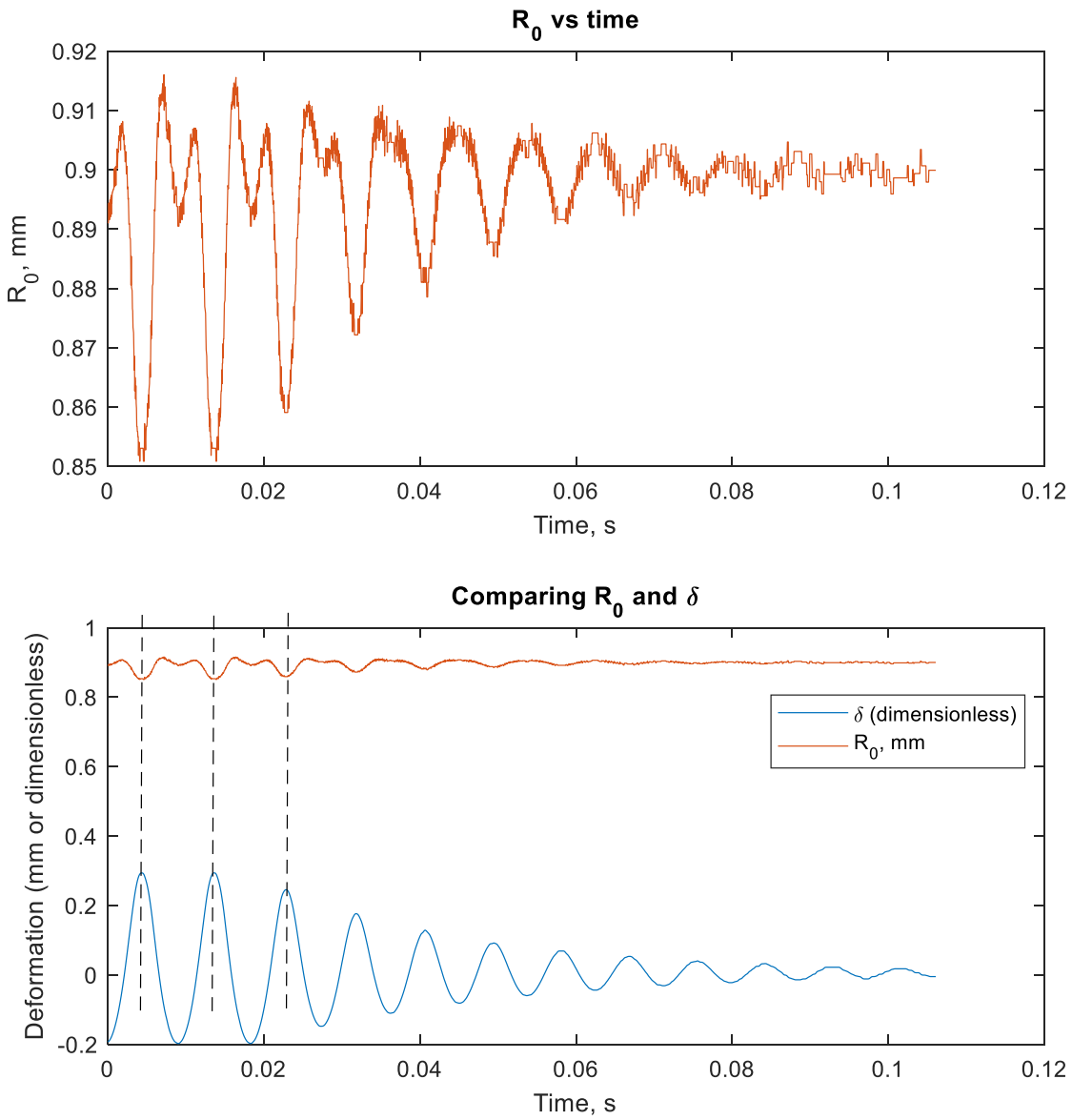

Figure 20. Change in characteristic radius R_0 as a function of time, compared to δ as a function of time to highlight correlation.

The evident variation in R_0 over time points to the droplet violating the ellipsoid assumption most severely at δ maxima (points of maximum oblateness). The dips in R_0 at those points indicate that at maximum oblateness, the droplet squashes and flattens out, leading to an ellipsoid with its characteristic height having less volume.

For the δ minima (points of greatest prolateness), variations in R_0 are of approximately 0.01mm magnitude. This is only slightly larger than the side length of a single pixel (0.0092-0.0095 mm depending on calibration), which suggests that the variation is functionally negligible. Only these points are thus used in Figure 21, which fits a parabola in a least-squares sense to each droplet volume-differentiated set of data in accordance with the expected quadratic relationship between droplet deformation amplitude and natural frequency shift as determined by Tsamopoulos and Brown [4].

It was observed in the datasets tabulated in the results that sometimes more than one point at the beginning of a given set had the same δ value; this is indicative of a steady-state oscillatory period being contained in the survey window along with the transient data. In the following plots, these are trimmed out in order to avoid weighting points that correspond to the driven oscillation; these are likely not representative of the free-decay behavior of the droplet and thus should not be considered in any interpretation. The least-squares fitting approach applied in Figure 21 would be biased by the presence of an extra point overlaying an existing one, so with these removed the fitting is conducted free of this influence and is more representative of the transient behavior.

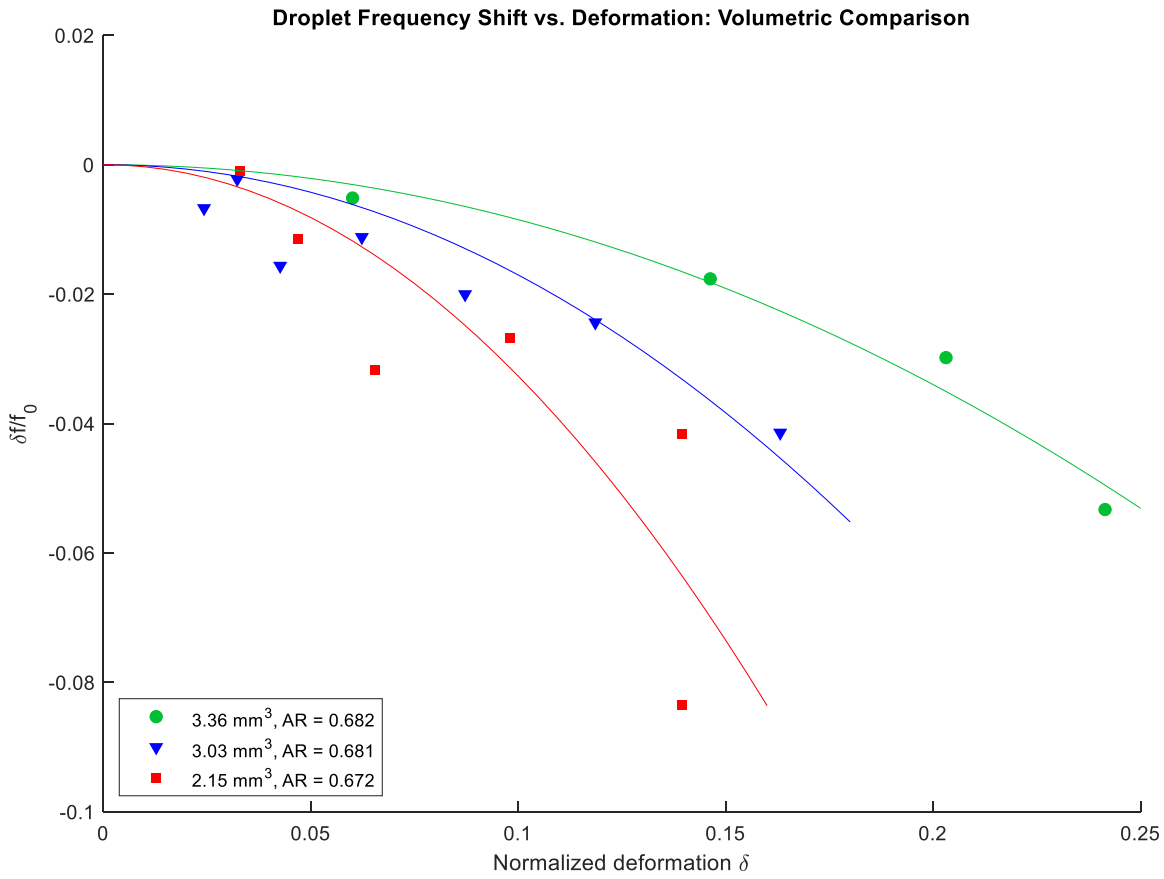

Figure 21. δ minima for three droplets of different volumes, with quadratic fits forced through the origin as proposed by Tsamopoulos and Brown [4].

A preliminary estimate of errors in fitting these curves to the present data is shown in Figure 22. The error bars were determined by MATLAB functions polyfit and polyval, which together estimate the standard deviation of the error in predicting a future observation at index x via polynomial fit P(x) using centering and scaling arguments.

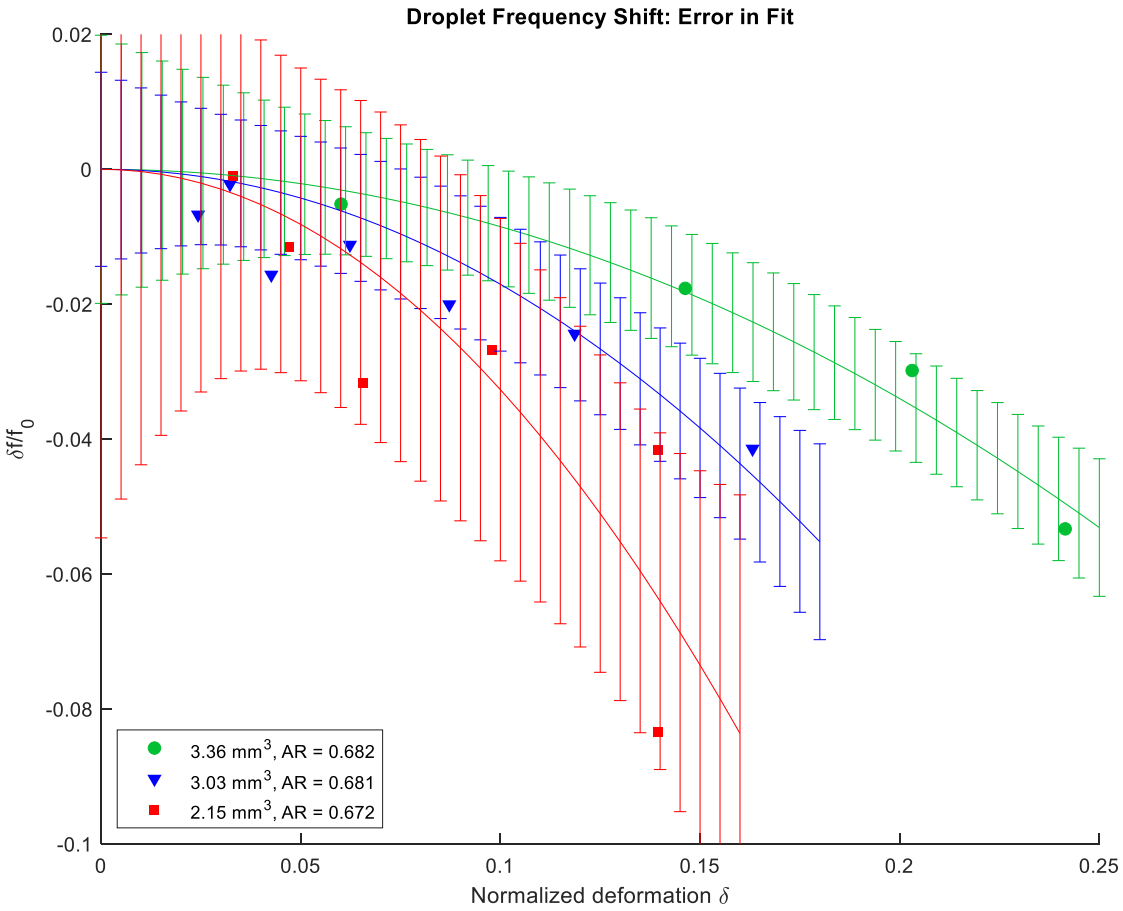

Figure 22. δ minima for three droplets of different volumes, with error bars illustrating estimated uncertainty in fit data.

The error bars shown above grow large in the cases of all three datasets at low deformations – this can be attributed to the significant scatter in the locations of found peaks in that range. The observation that one of the low-deformation points for the 3.03 mm^3 droplet falls outside of the bars is indicative of the fact that the bars only represent one standard deviation; there exists a 31.7 percent chance for a given observed data point to be outside these bounds, and we see that realized in Figure 22.

As a further treatment, the bounding envelopes present in Figure 23 that are used to generate the error bars in Figure 24 were visually estimated – they have no actual statistical backing but give the reader another means of visualizing the uncertainty present in each dataset.

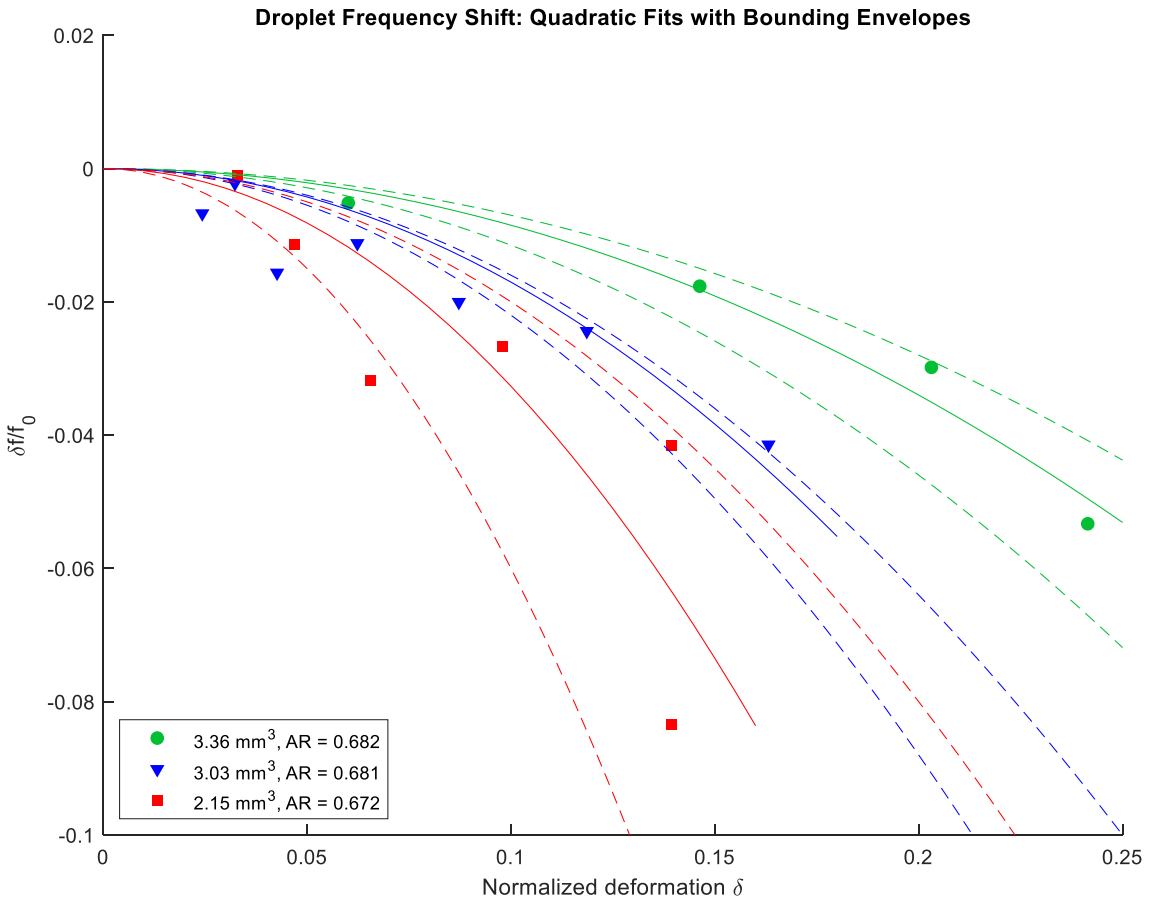

Figure 23. δ minima for three droplets of different volumes, with visually estimated bounding envelopes within which most points fall.

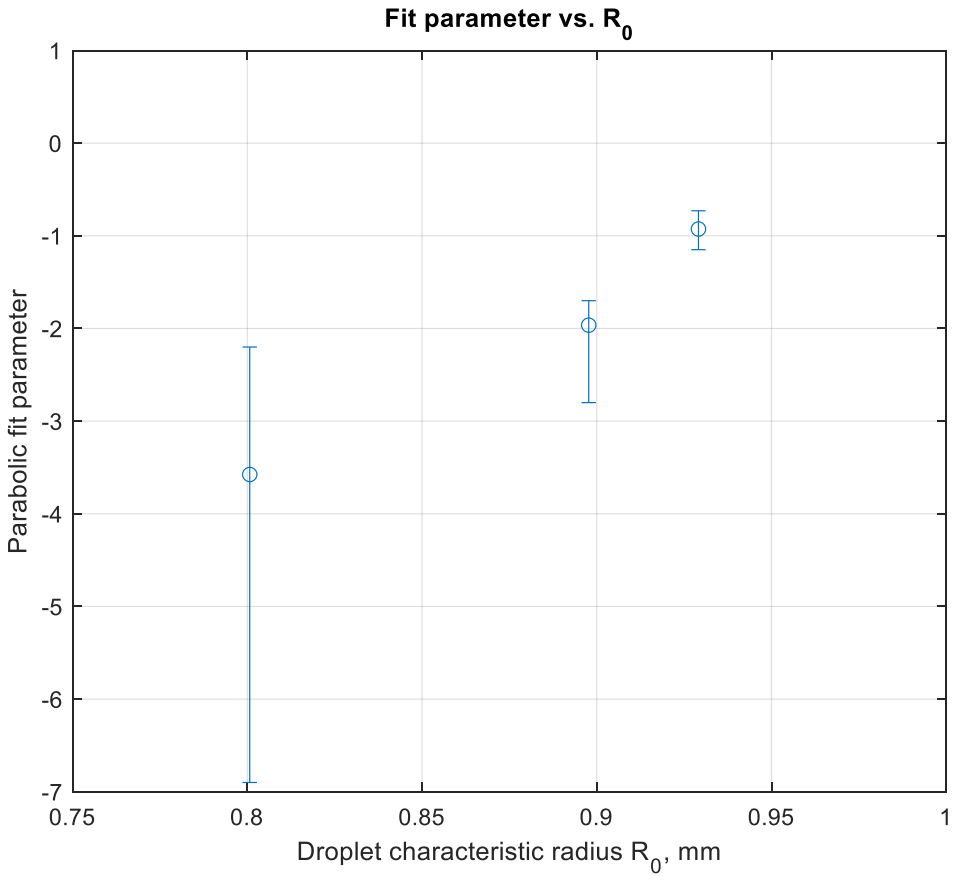

Figure 24. Parabolic fit coefficient vs. characteristic R_0 for three droplets, with error bars defined by bounding envelopes.

Interpretation of Results: Zero-to-Zero Data

Applying the zero-to-zero method of measuring periods allows for the isolation of data gathered from the prolate deformations from that gathered from the oblate deformations. As was demonstrated by the test of the ellipsoid assumption shown in Figure 20, droplets subject to large oscillations using the acoustic levitator apparatus of this study hew much more closely to the ellipsoid assumption in the prolate phase of their oscillations. It is thus beneficial to consider the period data from the prolate phases alone, although any error in δ will be carried through the doubling necessary to

get full period data. Figure 18 illustrates the apparently nearly constant time the droplet spends in the oblate phase, even at high deformation; the frequency shift for the data maxima is minimal for all three shown droplets. This feature of the oscillation is given theoretical grounding by Tsamopoulos and Brown, recreated in numerical simulation by Foote and explored further by Basaran [2], [4], [8]. The zero-to-zero method of finding oscillatory period allows for isolation of the period data from the prolate phase. This is done, and the results are shown in Figure 25 with the same quadratic least-squares fit as was applied to the peak-to-peak data.

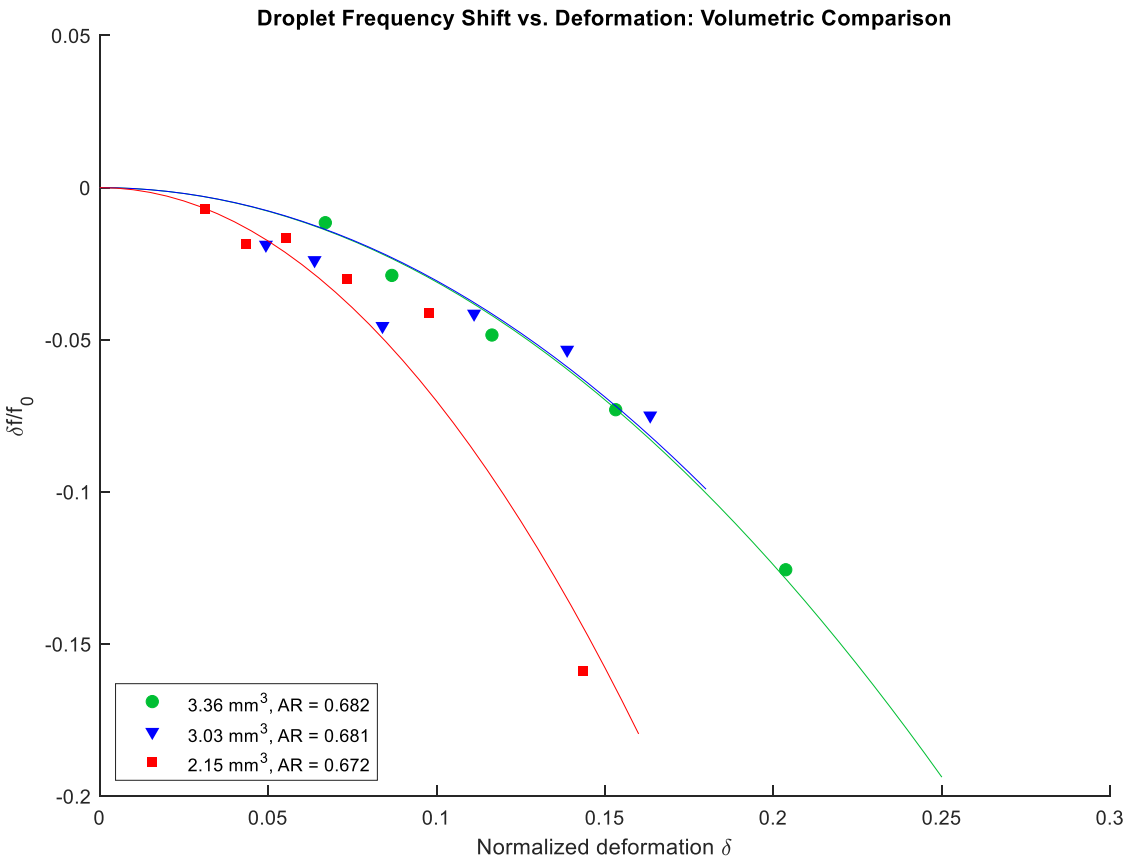

Figure 25. δ minima data for three droplets of different volumes with parabolic fit lines. Data obtained via zero-to-zero frame counting.

The error-bounding method applied in Figure 22 to the peak-to-peak data is applied once more to the zero-to-zero data, shown in Figure 26.

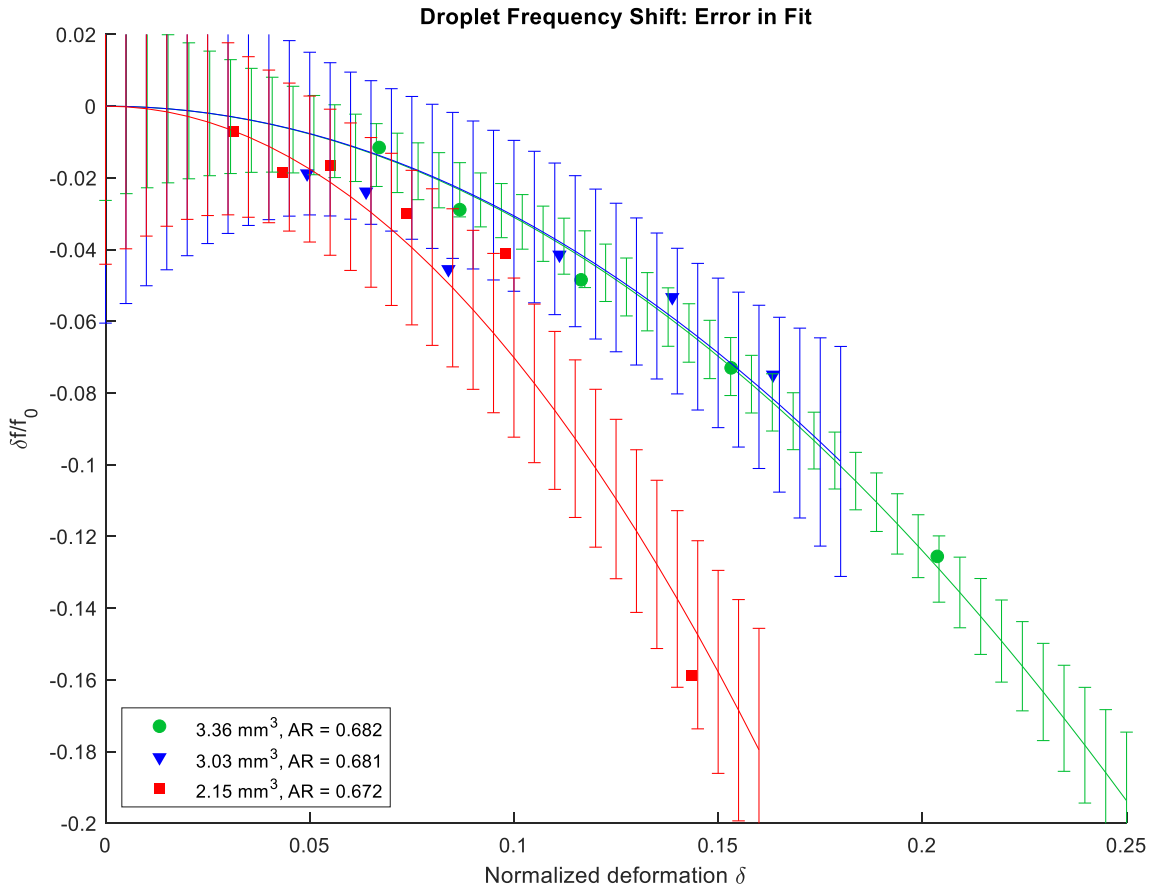

Figure 26. δ minima for three droplets of different volumes, with error bars illustrating estimated uncertainty in fit. Data obtained via zero-to-zero frame counting.

Given that the two larger droplets shown in Figure 26 are closer together in size than either is to the smallest one, this result appears to be more sensible than that shown in Figure 22. It is logical that a droplet only approximately two thirds of the size of the other two would behave significantly differently than either larger one. This suggested

relationship is at least superficially correlated by the following Figures 27 and 28, in which the bounding-envelope treatment introduced in Figures 23 and 24 is applied to this zero-to-zero data.

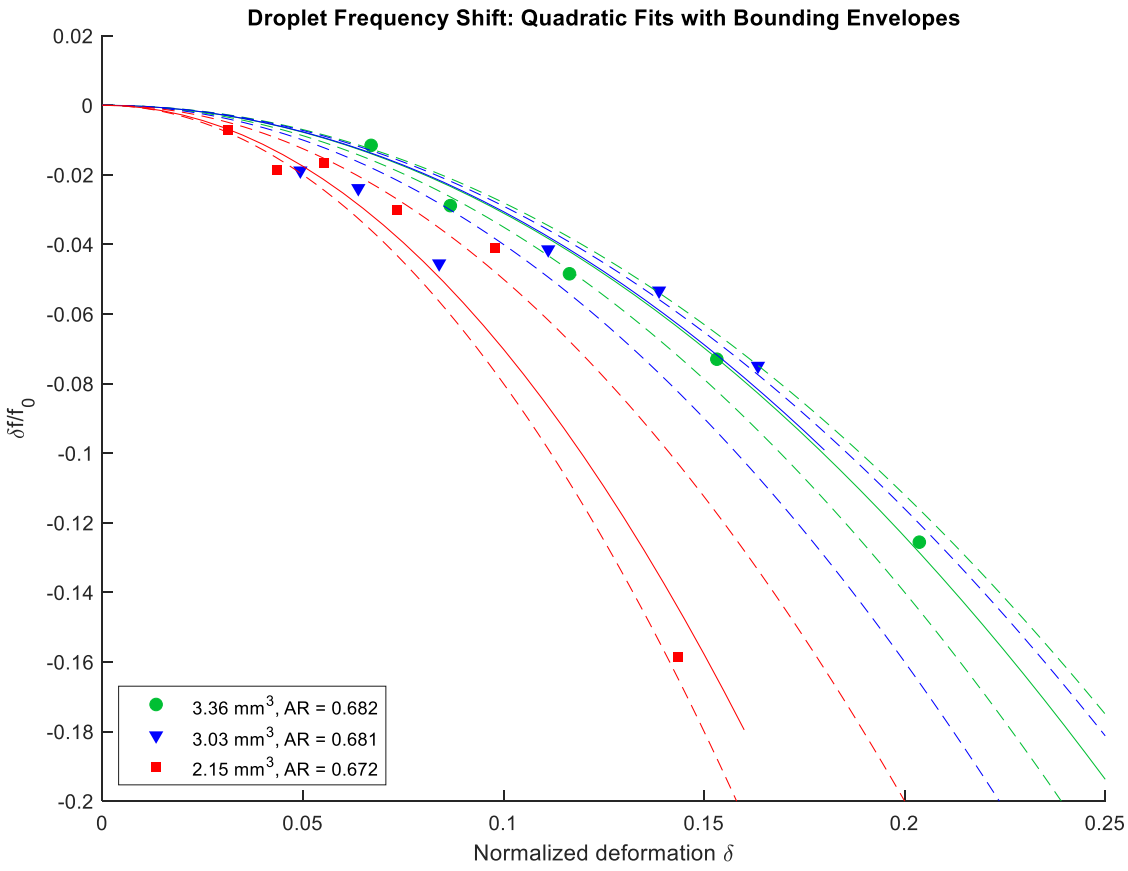

Figure 27. δ minima for three droplets of different volumes, with visually estimated bounding envelopes within which most points fall.

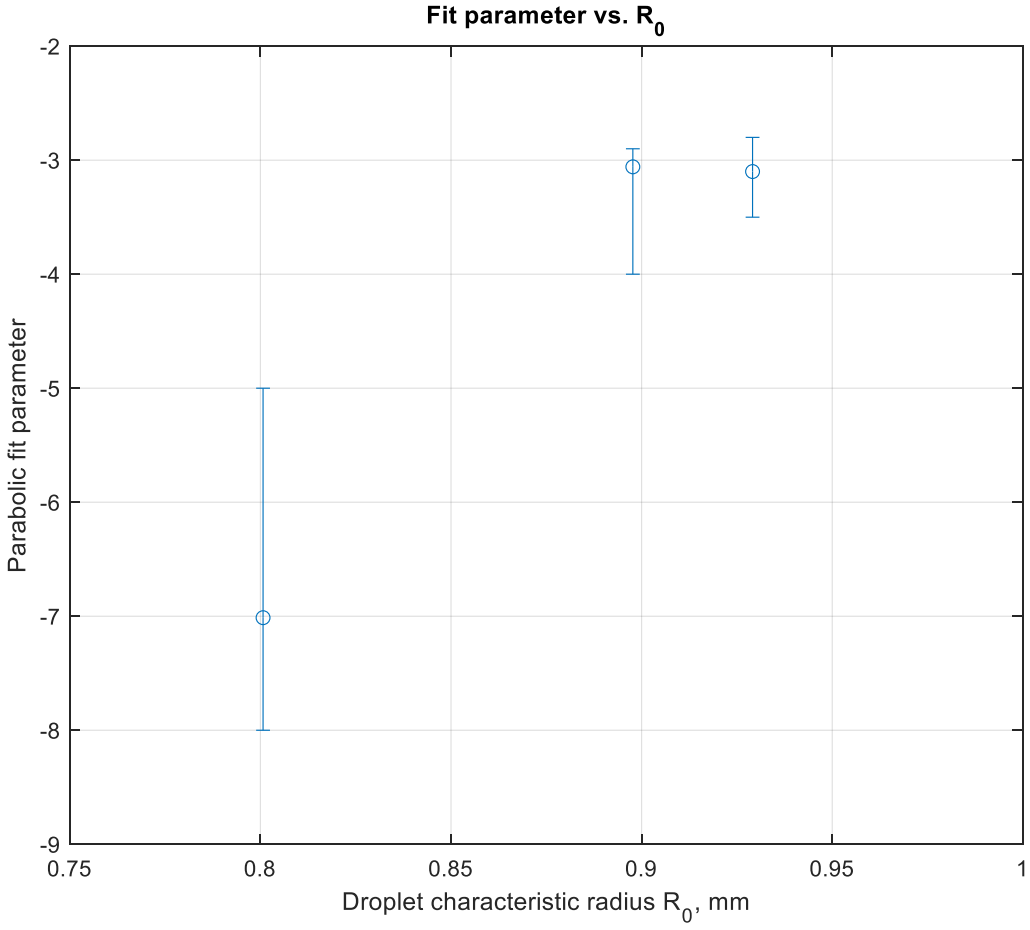

Figure 28. Parabolic fit coefficient vs. characteristic R_0 for three droplets, with error bars defined by bounding envelopes.

Since the "frequency shifts" studied in Figures 25 through 28 are based on only half of the period of each oscillation, they cannot be used to directly predict the behavior of smaller or larger oscillating droplets without further characterization of the droplet oblate-phase behavior. Since conducting this characterization was not within the scope of this study, understanding the nature of oscillations for which the ellipsoid assumption is valid throughout (namely, most oscillations used to actually study

material thermophysical properties, which are relatively smaller) is aided by examining the prolate phase in isolation.

Aspect Ratio Observations

In the peak-to-peak survey of droplets with different aspect ratios, a very tentative correlation between resting aspect ratio and natural frequency appears to be shown, with droplets of lower aspect ratio (more flattened while at rest) showing small-deformation natural frequencies higher than the Rayleigh natural frequency. This may be due to the frequency-splitting effect theoretically explored by Cummings and Blackburn, with the highest-amplitude frequency shifting up with greater asymmetry; however, this data is not nearly well enough differentiated to give any sort of statistical confidence in the theory. Furthermore, it is not noticeably supported by the zero-to-zero data for the minima, although the maxima do seem to show a trend with the δ maxima of the droplet of smallest aspect ratio depressing more with larger δ than for the other droplets.

Principal Sources of Error

The several sources of experimental uncertainty in this problem can be grouped into two major categories: errors in observed frequency shift $\delta f/f_0$ and deformation δ, which contribute to data scatter, and errors in the normalization frequency, which effectively translate the data shown in every $\delta f/f_0$ vs δ plot upward or downward. Neither subset can be discounted.

Error in δ

Understanding uncertainty in δ requires investigating how δ was acquired and what input quantities were necessary. It was found by analysis of the aspect ratio, which relies on height and width measurements of the droplet. These have a base uncertainty of one pixel-length, or slightly under 0.01 mm depending on the size of the camera field of view for a given run. Further uncertainty is introduced by the exceptionally high value used in thresholding each greyscale frame into a binary matrix (so chosen because the high contrast of the greyscale images allows it). However, a calculation of the height and width of a given frame using the high threshold and using a lower one (220 vs 250, with values ranging from 0 to 255) demonstrates that this variation is limited to two pixels and is often less; therefore, height and width values are measured by the program to a precision of +/- 0.019 mm. Defining aspect ratio as height divided by width, this uncertainty also results in a maximum aspect ratio variation of +/- 0.015; the effect on δ, once propagated through, is +/- 0.01. It is worth noting here that the visual measurement of the droplets was also conducted to a precision of 0.02 mm.

Error in frequency shift, peak-to-peak measurement

Uncertainty in the frequency shift $\delta f / f_0$ is more difficult to quantify because it relies on the accuracy of the MATLAB image processing code's detection of maxima and minima. By visual inspection, the small-scale choppiness of time-domain δ data, an effect of the sampling rate (the camera frame rate), introduces an approximate error of +/- 0.0005 seconds to the measurement of time between peaks. At typical frequency

ranges, this results in a variation in measured frequency of approximately +/- 2 hertz, translating to a dimensionless $\delta f / f_0$ variation of about +/- 0.02.

Error in natural frequency f_0

The Rayleigh natural frequency measurement's uncertainty depends on constituent initial volume fraction, droplet size and ambient temperature. The uncertainty in initial volume fraction is on the order of +/- 0.03, resulting in an error in f_0 of +/- 0.7 hertz. Visually determined initial droplet dimensional measurement uncertainty contributes a maximum f_0 error of +/- 2 Hz, for the smallest droplets tested, and the effect of changing temperature (variation +/- 1°C) is negligible. The effect of these errors is seen in the accuracy of the polynomial fit; if the data clearly reaches 0 deformation at a frequency that is not the calculated f_0 value, a quadratic fit through the plot origin will be distorted.

Error in frequency shift, zero-to-zero measurement

A further ramification of natural frequency error becomes apparent in applying the zero-to-zero period measurement method. If the droplet's dimensional measurements are inaccurate, the measured and actual resting aspect ratio of the droplet will differ; this manifests as the droplet appearing to deform about a nonzero resting δ. Period measurements from zero to zero thus result in distorted data. This distortion can be seen in Figure 29.

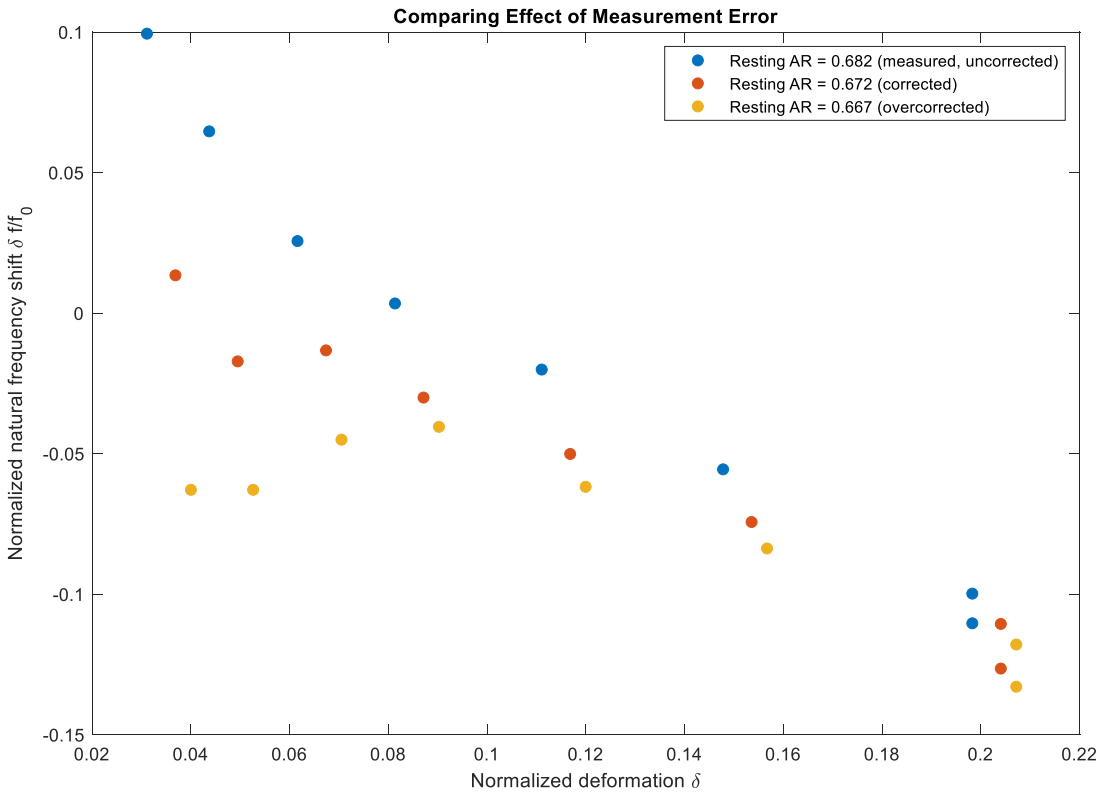

Figure 29. A comparison of the effect of varying the resting aspect ratio on frequency shift data.

This figure illustrates the necessity of correcting for aspect ratio uncertainty when using this measurement method. In this study, the correction is made by fitting a sine wave to the small-amplitude oscillations near the end of the observed time-domain signal and subtracting that sine wave's offset from the δ data. This centers the oscillation about $\delta = 0$ and compensates for measurement error.

Impact of Framerate

The reader may have noticed the phenomenon of more than one data point in some of the datasets included in this thesis having the same values for $\delta f/f_0$, δ or both. This is an effect of the framerate; there being only two to three hundred frames per oscillatory period forces only relatively large changes to be observed. However, it typically also indicates that, for the datasets where the effect is present, a steady-state driven oscillatory peak or two made it into the video snippet used to create the dataset. This was described above in relation to trimming down datasets before applying the parabolic least-squares fit. The phenomenon of there being more than one of a very specific value (accurate out to 4+ decimal places) in a given dataset serves to highlight the relatively limited sampling rate that even 27,000 frames per second represents for oscillations on the order of 100 hertz. The frequencies are not being measured to that precision; those are calculated values that just happen to have several decimal places to them.

Comparing to Prior Results

The sum of potential errors discussed above indicates that further data collection and refinement of the experimental setup is necessary to develop statistical confidence in these results. However, preliminary comparisons can be drawn between these results and those of Trinh and Wang [16]. They illustrate the same trend: the natural frequency of an oscillating droplet depresses more at high deformation amplitude for a small droplet than for a large one. The experimental setup and conditions of the test are very different, with Trinh and Wang having conducted their evaluation on neutrally

buoyant droplets floating in liquid; however, both methods used acoustic levitation and so the forces applied by the locating field are similar in nature if not in magnitude. Any quantitative comparison between the two methods is dubious in its utility due to the small number of points in each data set and the relatively large uncertainties present in the data of this study. However, each offers its own advantages, with Trinh and Wang's method reducing the influence of the levitation on droplet shape and the in-air method explored in this thesis more accurately representing the conditions under which material property characterization studies are conducted.

Conclusions

Experimental apparatus suitability for further testing

- Acoustic levitator utility for analyzing behavior of oscillating droplets has been demonstrated, with analysis of a range of droplet sizes and careful control over oscillatory deformation amplitude possible
- Media used are too viscous to obtain many data points, necessitating repeated trials with different droplets of similar initial size due to water evaporation
- Volatility of water and dynamic composition of tested mixture are suboptimal for conducting testing wherein measurement of droplet oscillatory behavior cannot immediately follow droplet insertion; they necessitate calculation of mixture thermophysical properties at the time of the test and represent an additional potential source of experimental error
- Image processing code returns data that appear to resolve oscillation characteristic of interest, but has no ability to isolate or characterize individual oscillatory modes if several are present

Obtained results

- Data appear to show size dependency of droplet deformation frequency shift at high oscillation amplitudes, but more is needed to develop statistical significance
- There appears to be no influence of droplet aspect ratio (a proxy for levitation pressure) on frequency shift at high oscillation amplitudes, but the present data set does not contain enough data of suitable parameters to observe variable aspect ratio in isolation

- Overall error in data collection and processing (combination of relatively low resolution, high droplet damping rate and attendant uncertainty in deformation peak location) leads to significant scatter in data
- Measuring frequency shift with δ variation using zero-to-zero method allows for isolation of data wherein droplet conforms closely to ellipsoid assumption, but does not accurately return frequency data because the amounts of time droplets spends in prolate and oblate phases of large-amplitude oscillation are not equal

Future Work

Continued application of acoustic levitation techniques to characterizing the relationship tentatively observed within this study should consist of more data being collected with an effort made to minimize controllable error. Refinement of the image-processing code and determination of means of reducing the surface tension and viscosity characteristics of the droplets studied would both be worthwhile steps to take. This could consist either of putting a laser incident on the sample and heating it in this manner or of raising the ambient temperature about the levitator (read: situating it in an oven). The effects of elevated temperature on the resonance characteristics of the levitator would require investigation, and a sample material with low enough evaporation rate in the elevated temperature envelope to take useful data would be necessary. Testing on a sample of nonnegligible evaporation rate has a real benefit to the rate of data collection, provided that the droplet's composition is static; it would theoretically allow for several datasets at different sizes to be taken from one volume-varying droplet.

Further characterization of the effect of acoustic pressure on this relationship is also necessary. Some combination of the droplet being increasingly distorted from the spherical form and the acoustic levitation force's own effect on the oblate-prolate oscillations will almost certainly begin to dominate the intended effect and determining how to correct for that is necessary to gather accurate data from acoustic testing.

References

[1] J. W. Strutt, “VI. On the capillary phenomena of jets,” *Proceedings of the Royal Society of London*, vol. 29, no. 196–199, pp. 71–97, Jan. 1879, doi: 10.1098/rspl.1879.0015.

[2] G. Foote, “A numerical method for studying liquid drop behavior: Simple oscillation,” *Journal of Computational Physics*, vol. 11, no. 4, pp. 507–530, Apr. 1973, doi: 10.1016/0021-9991(73)90135-6.

[3] C. T. Alonso, “The dynamics of colliding and oscillating drops,” University of California Berkeley; Lawrence Berkeley Laboratory, 19820066620, Jan. 1974.

[4] J. A. Tsamopoulos and R. A. Brown, “Nonlinear oscillations of inviscid drops and bubbles,” *Journal of Fluid Mechanics*, vol. 127, pp. 519–537, 1983, doi: 10.1017/S0022112083002864.

[5] E. Becker, W. J. Hiller, and T. A. Kowalewski, “Experimental and theoretical investigation of large-amplitude oscillations of liquid droplets,” *Journal of Fluid Mechanics*, vol. 231, pp. 189–210, 1991, doi: 10.1017/S0022112091003361.

[6] H. Lamb, “On the Oscillations of a Viscous Spheroid,” *Proceedings of the London Mathematical Society*, vol. s1-13, no. 1, pp. 51–70, Nov. 1881, doi: 10.1112/plms/s1-13.1.51.

[7] A. Prosperetti, “Free oscillations of drops and bubbles: the initial-value problem,” *Journal of Fluid Mechanics*, vol. 100, no. 2, pp. 333–347, 1980, doi: 10.1017/S0022112080001188.

[8] O. A. Basaran, “Nonlinear oscillations of viscous liquid drops,” *Journal of Fluid Mechanics*, vol. 241, pp. 169–198, 1992, doi: 10.1017/S002211209200199X.

[9] D. L. Cummings and D. A. Blackburn, “Oscillations of magnetically levitated aspherical droplets,” *Journal of Fluid Mechanics*, vol. 224, pp. 395–416, 1991, doi: 10.1017/S0022112091001817.

[10] P. V. R. Suryanarayana and Y. Bayazitoglu, “Effect of static deformation and external forces on the oscillations of levitated droplets,” *Physics of Fluids A: Fluid Dynamics*, vol. 3, no. 5, pp. 967–977, May 1991, doi: 10.1063/1.857974.

[11] I. Egry, G. Lohoefer, and G. Jacobs, “Surface Tension of Liquid Metals: Results from Measurements on Ground and in Space,” *Physics Review Letters*, vol. 75, no. 22, pp. 4043–4046, Nov. 1995, doi: 10.1103/PhysRevLett.75.4043.

[12] T. Shi and R. E. Apfel, “Oscillations of a deformed liquid drop in an acoustic field,” *Physics of Fluids*, vol. 7, no. 7, pp. 1545–1552, Jul. 1995, doi: 10.1063/1.868541.

[13] E. H. Trinh, P. L. Marston, and J. L. Robey, “Acoustic measurement of the surface tension of levitated drops,” *Journal of Colloid Interface Science*, vol. 124, no. 1, pp. 95–103, Jul. 1988, doi: 10.1016/0021-9797(88)90329-3.

[14] Y. Tian, R. G. Holt, and R. E. Apfel, “A new method for measuring liquid surface tension with acoustic levitation,” *Review of Scientific Instruments*, vol. 66, no. 5, pp. 3349–3354, May 1995, doi: 10.1063/1.1145506.

[15] E. H. Trinh, “Compact acoustic levitation device for studies in fluid dynamics and material science in the laboratory and microgravity,” *Review of Scientific Instruments*, vol. 56, no. 11, pp. 2059–2065, Nov. 1985, doi: 10.1063/1.1138419.

[16] E. Trinh and T. G. Wang, “Large-amplitude free and driven drop-shape oscillations: experimental observations,” *Journal of Fluid Mechanics*, vol. 122, pp. 315–338, 1982, doi: 10.1017/S0022112082002237.

[17] J. G. McDaniel and R. G. Holt, “Measurement of aqueous foam rheology by acoustic levitation,” *Physical Review E*, vol. 61, no. 3, pp. R2204–R2207, Mar. 2000, doi: 10.1103/PhysRevE.61.R2204.

[18] A. J. A. van der Wyk, “Viscosity of Binary Mixtures,” *Nature*, vol. 138, no. 3498, pp. 845–846, Nov. 1936, doi: 10.1038/138845b0.

[19] S. Arrhenius, “The Viscosity of Aqueous Mixtures,” *Zeitschrift für Physikalische Chemie*, vol. 1, p. 285, 1887.

[20] K. A. Connors and J. L. Wright, “Dependence of surface tension on composition of binary aqueous-organic solutions,” *Analytical Chemistry*, vol. 61, no. 3, pp. 194–198, Feb. 1989, doi: 10.1021/ac00178a001.

[21] N. G. Tsierkezos and I. E. Molinou, “Thermodynamic Properties of Water + Ethylene Glycol at 283.15, 293.15, 303.15, and 313.15 K,” *Journal of Chemical Engineering Data*, vol. 43, no. 6, pp. 989–993, Nov. 1998, doi: 10.1021/je9800914.

[22] Koichiro. Nakanishi, Tadao. Matsumoto, and Mitsuyoshi. Hayatsu, “Surface tension of aqueous solutions of some glycols,” *Journal of Chemical Engineering Data*, vol. 16, no. 1, pp. 44–45, Jan. 1971, doi: 10.1021/je60048a010.

[23] J. J. Jasper, “The Surface Tension of Pure Liquid Compounds,” *Journal of Physical and Chemical Reference Data*, vol. 1, no. 4, pp. 841–1010, Oct. 1972, doi: 10.1063/1.3253106.

[24] M. Rusdi, Y. Moroi, H. Nakahara, and O. Shibata, “Evaporation from Water−Ethylene Glycol Liquid Mixture,” *Langmuir*, vol. 21, no. 16, pp. 7308–7310, Aug. 2005, doi: 10.1021/la040134g.

[25] J. Kremer, A. Kilzer, and M. Petermann, “Simultaneous measurement of surface tension and viscosity using freely decaying oscillations of acoustically levitated droplets,” *Review of Scientific Instruments*, vol. 89, no. 1, p. 015109, Jan. 2018, doi: 10.1063/1.4998796.

[26] D. Langstaff, M. Gunn, G. N. Greaves, A. Marsing, and F. Kargl, “Aerodynamic levitator furnace for measuring thermophysical properties of refractory liquids,” *Review of Scientific Instruments*, vol. 84, no. 12, p. 124901, Dec. 2013, doi: 10.1063/1.4832115.

Appendix: Data Processing and Analysis Code

The following MATLAB programs were used for image processing, dynamic droplet compositional determination, surface tension calculation and observation of deformation-dependent oscillatory frequency shift.

Droplet Image Processing: Master Code

```
%% Image Processing: Acoustically-Levitated Oscillating Droplet

% 2019, Courtland Priest

% Reads video file of droplet and finds deformation as a function of
time,
% returning frequency error plotted against the deformation parameter
with
% facility to write to a .csv file. Determines deformation versus
frequency
% shift for each oscillatory period using peak-to-peak method and also
% finds frequency shift vs. deformation based on half-periods,
measured
% from zero to zero for delta maxima and minima.

close all; clear all; clc;

% Input video file name and path
path='C:\Users\court\OneDrive\Desktop\MATLAB\Research 19\12-4-19
Testing\';
filename='12.4.19107.8Hz2800mV_C001H001S0001.mp4';

% Video frame rate
fs = 27000;

% Initial volume fraction of ethylene glycol
initvfetg = 0.5;

% Read in video file
videofile=strcat(path,filename);
mov=VideoReader(videofile);
nFrames = mov.NumFrames;

% Edge-detection threshold value
Ithresh = 250;

% Camera field-of-view parameters, pixel length and area
fov = [3.6021 3.6021];
pix = [384 384];
pxarea = (fov(1)/pix(1))^2;
pxlength = sqrt(pxarea);
```

```
% Preallocate I matrix
Imat = zeros(384,384,3);

% Convert each frame of video to binary, dilate/erode image to remove
% central transparency artifact
for i = 1:nFrames
    Frame=read(mov, i);

    tmp = double(Frame(:,:,1));
    tmp = 255-tmp;

    I = tmp > Ithresh;
    SE = strel('disk',50);
    I2 = imclose(I,SE);

    px(i) = sum(I2(:) == 1);
    Imat(:,:,i) = I2;
end

% Preallocate for droplet image boundary data
lbnd = zeros(1,length(nFrames));
rbnd = zeros(1,length(nFrames));
ubnd = zeros(1,length(nFrames));
dbnd = zeros(1,length(nFrames));

% Find highest, lowest, leftmost and rightmost points on droplet
regardless
% of shape
for k = 1:nFrames
    lbnd(k) = find(any(Imat(:,:,k),1),1);
    rbnd(k) = find(any(Imat(:,:,k),1),1,'last');
    dbnd(k) = find(any(Imat(:,:,k),2),1);
    ubnd(k) = find(any(Imat(:,:,k),2),1,'last');
end

% Set droplet height and width as functions of time, characteristic
radius
% of equivalent-volume sphere as function of time, and approximate
resting
% value for such (note: ellipsoid assumption introduced here)
height = (ubnd-dbnd)*pxlength;
width = (rbnd-lbnd)*pxlength;
r0 = ((height/2).*(width/2).^2).^(1/3);
r0end = mean(r0(end-500:end));

% Define vector of points in time
t = (1:nFrames)/fs;

%% Calculation of surface tension
% Calculate mixture surface tension using dimensional measurements,
% temperature and initial volume fraction of ethylene glycol

% Input droplet measured dimensions immediately after deployment and
after
% testing; input temperature observed on thermocouple
initw = 2.19;
```

```
inith = 1.45;
finalw = 2.11;
finalh = 1.44;
T = 18.4;

[rho, xetg] =
compositionOverTime(initw,inith,finalw,finalh,initvfetg);
sigma0 = getSigma(xetg,T,5.2);
volume = (4/3)*pi*(finalw/2)^2*(finalh/2)/1000;
volumeinitial = (4/3)*pi*(initw/2)^2*(inith/2)/1000;
mass = rho*volume; %in g

% Calculate Rayleigh natural frequency based on droplet final mass and
% surface tension
normf = sqrt(8*sigma0/(3*pi*mass));

%% Calculation of deformation parameter

delta = getDelta(height,width,finalh,finalw);

%% Fit parameterized sine wave to small-amplitude delta function
% This sets the oscillation to be about zero (eliminates offset error)

a = t(end-500:end);
b = delta(end-500:end);
sineParams = sineFit(a,b);

% Sinusoid characteristic parameters
offset = sineParams(1);
amp = sineParams(2);
freq = sineParams(3);
phi = sineParams(4);

% Can overplot parameterized sine onto delta data to check accuracy
sinewave = amp*sin(2*pi*freq*a + phi) + offset;

% Delta correction
delta = delta - offset;

%% Zero-finding in delta
% Finds frequency error as a function of delta using locations of
delta
% zeros in time

[minferrzz, maxferrzz] = zeroFinder(t,delta,normf,nFrames,fs);

%% Peak-finding in delta
% Finds delta maxima/minima indices (see function code for more
information)

[minidx, maxidx, pkmins, pkmaxs] = peakFinder(t,delta);

%% Adjustment of vector length
% From here: minferrzz/maxferrzz are zero-to-zero frequency shift for
delta
% minima/maxima; minferrpp/maxferrpp are the same for peak-to-peak
% measurements
```

```
if length(minferrzz)>length(minidx)
    minferrzz = minferrzz(1:length(minidx));
end

if length(maxferrzz)>length(maxidx)
    maxferrzz = maxferrzz(1:length(maxidx));
end

%% Calculation of frequency error as a function of delta

% Calculates differences between peak maxima and minima (two loops
because
% there may be different numbers of each)
for k = 1:length(maxidx)-1
    pkdiffmax(k) = abs(maxidx(k) - maxidx(k+1));
end
for k = 1:length(minidx)-1
    pkdiffmin(k) = abs(minidx(k) - minidx(k+1));
end

% Finds delta values corresponding to peak maxima and minima -
absolute
% value of minima taken so all points plot with one sign (direct
comparison)
maxes = delta(pkmaxs);
mins = abs(delta(pkmins));

% Transient interval: defines delta values to include (typically above
about
% 0.05) - use to trim out noisy low-amplitude data
tint = [1:8];

% Returns maxima and minima indicated by trange
maxdeltaout = maxes(tint);
mindeltaout = mins(tint);

% Calculates frequency difference from Rayleigh natural frequency,
% normalized about 0

maxferrpp = fs./pkdiffmax(tint)/normf - 1;
minferrpp = fs./pkdiffmin(tint)/normf - 1;

minferrzz = minferrzz(tint);
maxferrzz = maxferrzz(tint);

% Plots maxima and minima against frequency error from Rayleigh
frequency
figure; hold on
scatter(mindeltaout, minferrpp)
scatter(maxdeltaout, maxferrpp)
title('Oscillation frequency vs deformation amplitude')
xlabel('Droplet width variation over unstrained width')
ylabel('Natural frequency, normalized')

%% Subplots
```

```
% Subplots to show alignment of dips in calculated r0 with delta
maxima data

figure

subplot(2,1,1)
plot(t,r0,'color',[0.8500    0.3250    0.0980])
xlabel('Time, s')
ylabel('R_0, mm')
title('R_0 vs time')

subplot(2,1,2)
plot(t,delta,t,r0)
xlabel('Time, s')
ylabel('Deformation (mm or dimensionless)')
title('Comparing R_0 and \delta')
legend('\delta (dimensionless)','R_0, mm')

%% Write to CSV (peak-to-peak)
% Writes to CSV: columns as follows
% 1. Frequency values measured as difference between maxima
% 2. Frequency error of maxima
% 3. Maximum delta values
% 4 through 6: 1 through 3 but for minima

writematrix([(fs./pkdiffmax(tint))' maxferrpp' maxdeltaout' ...
    (fs./pkdiffmin(tint))' minferrpp'
mindeltaout'],'dec488.7Hzdelta.csv','FileType','text')

%% Write to CSV (zero-to-zero)
% .csv file format same as for peak-to-peak files

writematrix([(fs./pkdiffmax(tint))' maxferrzz' maxdeltaout'...
    (fs./pkdiffmin(tint))' minferrzz'
mindeltaout'],'dec5111Hzdeltaalt.csv','FileType','text')
```

Droplet Thermophysical Property Calculations

Used during testing to calculate droplet Rayleigh natural frequency based on initial measured dimensions and 50/50 water/ethylene glycol mix.

```
%% Mole fraction, density, volume calculations

% 2019, Courtland Priest

% Calculates mole fractions of ethylene glycol and water in mixture,
% and total mixture density and droplet volume given dimensions

vfrac1 = 0.5; %ethylene glycol
vfrac2 = 1 - vfrac1;

% Molar masses
mmwater = 18.01; %g/mol
```

```
mmetg = 62.07;

% Densities
rhowater = 0.997; %g/cm^3
rhoetg = 1.113;

% Density calculation
rhomix = vfrac1 * rhoetg + vfrac2 * rhowater;

% Molar volume of water and ethylene glycol
molvolw = mmwater/rhowater; %cm^3/mol
molvoletg = mmetg/rhoetg;

% Number of moles of each in one mole of mixture
nmolsetg = vfrac1/molvoletg;
nmolsw = vfrac2/molvolw;

% Mole fraction of ethylene glycol
xetg = nmolsetg/(nmolsw+nmolsetg);

%% Get surface tension
sigmix = getSigma(0.5, 18.6, 5.2);

% Volume calc from droplet axis msmts. (assume oblate spheroid)
% Dimensions in mm
h = 1.7; %mm
w = 2.6;%mm
rho = rhoetg; %g/cm^3;
sig0 = sigmix; %mN/m %g/s

vol = (4/3) * pi * (w/2)^2 * h/2 /1000; %cm^3
mass = rho*vol; %g
f0 = sqrt(8*sig0/(3*pi*mass));
```

Droplet Compositional Change Calculation

Computes change in mole fraction of ethylene glycol due to water evaporation over the course of the evaluation of a single droplet.

```
function [rhomix,xetg] =
compositionOverTime(initw,inith,finalw,finalh,vfracetg)

% 2019, Courtland Priest

% Determine change in composition over course of experimental
evaluation,
% assuming that water is the only evaporating species

% Calculate volume change
initvol = (4/3)*pi*(initw/2)^2*(inith/2);
finalvol = (4/3)*pi*(finalw/2)^2*(finalh/2);
deltavol = finalvol - initvol; %mm^3
```

```
% Initial volume fractions
vfrac1 = vfracetg;
vfrac2 = 1 - vfrac1;

% Initial and final volumes of each constituent
initvwater = vfrac2*initvol;
initvetg = vfrac1*initvol;
finalvwater = initvwater + deltavol;
vf1final = initvetg/finalvol;
vf2final = finalvwater/finalvol;

% Constituent molar masses
mmwater = 18.01; %g/mol
mmetg = 62.07;

% Constituent densities
rhowater = 0.997; %g/cm^3
rhoetg = 1.113;

% Mixture final density
rhomix = vf1final * rhoetg + vf2final * rhowater;

% Molar volumes of constituents
molvolw = mmwater/rhowater; %cm^3/mol
molvoletg = mmetg/rhoetg;

% Number of moles in one mole of mixture
nmolsetg = vf1final/molvoletg;
nmolsw = vf2final/molvolw;

% Return new mole fraction ethylene glycol
xetg = nmolsetg/(nmolsw+nmolsetg);
```

Droplet Surface Tension Calculation

Computes the mixture's surface tension given input volume fraction of ethylene glycol, temperature measurement and sensor offset error (if present).

```
function sigmix = getSigma(xetg, measuredT, offset)

% 2019, Courtland Priest

% Returns surface tension of binary mixture of ethylene glycol and
water
% given mole fraction of ethylene glycol.

% Temperature dependence data obtained from "The Surface Tension of
Pure Liquid
% Compounds", Jasper (1973)
% Alpha and beta coefficients obtained from "Thermodynamics of Water
and
% Ethylene Glycol at...", Tsierkezos and Molinou (1998)
```

```
% Coefficients for temperature range between 20 and 30 degrees C - to
% generalize for more temperatures, refer to above texts for empirical
% coefficients

temperature = measuredT + offset;
x1 = xetg; %mole fraction of ethylene glycol
x2 = 1 - x1; %mole fraction of water

t = temperature - 20;

% Temperature dependence of surface tension determined from Jasper
tcoeff1 = -0.0890; %for EtG
tcoeff2 = -0.1514; %for water
sig1 = 47.70 + tcoeff1*t; %mN/m, EtG
sig2 = 72.80 + tcoeff2*t; %mN/m, water

% Coefficients alpha and beta linearly interpolated from
Tsierkezos/Molinou
% data (they only measured in increments of 10 degC)
alpha = 0.6912 + (t/10) * (0.7253 - 0.6912);
beta = 0.8810 + (t/10) * (0.8859 - 0.8810);

% Recovered from Connors et al. by way of Tzierkezos
sigmix = sig2 - (1 + (alpha*x2)/(1-beta*x2)) * x1 * (sig2 - sig1);
```

Computing δ Parameter from Aspect Ratio Data

Calculates δ from aspect ratio data for set of time-domain data (aspect ratio defined as droplet height divided by droplet width).

```
function [delta, restAR] = getDelta(height,width,finalh,finalw)
% Determine droplet aspect ratio as function of time as well as value
% immediately after test (resting state)

aspectrat = height./width;
restAR = finalh/finalw;

% Preallocate for Delta vector
Delta = zeros(1,length(aspectrat));

% Determine roots of cubic equation
for k = 1:length(aspectrat)
    DeltaRoots = roots([1 3 3 1-1/aspectrat(k)]);

    % Take real root (the other two will always be complex)
    Delta(k) = DeltaRoots(3);
end

% Determine and correct for droplet resting deformation from spherical
delta0 = roots([1 3 3 1-1/restAR]);
delta0 = delta0(3);
delta = filloutliers(real(Delta-delta0),'linear','mean');
```

Computing Deformation-Dependent Frequency Shift, Zero-to-Zero

Finds frequency shift as a function of deformation parameter δ using time between δ zeros. This half-period data is computed for δ maxima and minima.

```
function [minfreqerr, maxfreqerr] =
zeroFinder(t,delta,normf,nFrames,fs)
% Finds zeros of delta data, half-periods and then frequencies for
each
% half-period

% Find locations where data crosses x-axis
[zs, zidx] = data_zeros(t,delta);

% Set up empty vectors for appending
asczidx = [];
dsczidx = [];

% Assign delta values with indices zidx to temporary vector
temp = delta(zidx);

% Build vectors of indices corresponding to ascending and descending
zeros
for k = 1:length(temp)
    if temp(k) < 0
        asczidx = [asczidx k];
    else
        dsczidx = [dsczidx k];
    end
end

% Trim front of zero vector if first zero is ascending
if dsczidx(1) > asczidx(1)
    zs = zs(2:end);
end

% Find half-period values which enclose delta minima
for k = 1:2:length(zs)-1
    halfpermin(k) = zs(k+1)-zs(k);
end

% Find half-period values which enclose delta maxima
for k = 2:2:length(zs)-1
    halfpermax(k) = zs(k+1)-zs(k);
end

%Toss out zero values in each vector
halfpermin = halfpermin(halfpermin~=0);
halfpermax = halfpermax(halfpermax~=0);

%Compute projected full periods from half-period data
permins = 2*halfpermin;
permaxs = 2*halfpermax;
```

```
%Plots
figure
plot((1:nFrames)./fs,delta,(zidx(asczidx))./fs,zeros(1,length(asczidx)
),'*',...
    (zidx(dsczidx))./fs,zeros(1,length(dsczidx)),'o')
xlabel('Time, s')
ylabel('\delta')
legend('\delta: normalized width deformation','Ascending
zeros','Descending zeros')
title('Time-domain oscillation amplitude, highlighted zeros')

%Computes apparent frequency for each half-period enclosing delta
minima
%and delta maxima

minfreqs = 1./permins;
maxfreqs = 1./permaxs;

%Normalized against Rayleigh natural frequency
minfreqerr = (minfreqs-normf)./normf;
maxfreqerr = (maxfreqs-normf)./normf;
```

Locating Indices of δ Maxima and Minima

Finds indices of δ maxima and minima in time-domain oscillation data.

```
function [minidx, maxidx, pkmins, pkmaxs] = peakFinder(t,delta)
% Finds delta maxima and minima and indices thereof, plots with
markers

% Locate local maxima and minima
pkmins = islocalmin(delta, 'MinProminence', 0.02);
pkmaxs = islocalmax(delta, 'MinProminence', 0.02);

% Return indices of local maxima and minima
maxidx = find(pkmaxs);
minidx = find(pkmins);

% Plot delta with maxima and minima indicated
figure
ax = axes;
plot(ax,t,delta,t(pkmins),delta(pkmins),'*',t(pkmaxs),...
    delta(pkmaxs),'o')
xlabel('Time, s');
ylabel('\delta')
legend('\delta: normalized width deformation','Minima','Maxima')
title('Time-domain oscillation amplitude, highlighted minima and
maxima')
```